國 立 交 通 大 學

電子物理學系

碩士論文

含鐵超導材料 $FeSe_{1-\delta}$ 與銅摻雜之 $(Fe_{1-x}Cu_x)Se_{1-\delta}$ 的核磁共振研究

NMR study of Iron-based superconductor $FeSe_{1-\delta}$ and

Cu-doped $(Fe_{1-x}Cu_x)Se_{1-\delta}$

研 究 生：吳家慶

指導教授：楊本立　教授

中 華 民 國 九 十 九 年 七 月

含鐵超導材料 $\mathrm{FeSe}_{1-\delta}$ 與銅摻雜之 $(\mathrm{Fe}_{1-x}\mathrm{Cu}_x)\mathrm{Se}_{1-\delta}$ 的核磁共振研究

NMR study of Iron-based superconductor $\mathrm{FeSe}_{1-\delta}$ and Cu-doped $(\mathrm{Fe}_{1-x}\mathrm{Cu}_x)\mathrm{Se}_{1-\delta}$

研 究 生：吳家慶　　　　　Student：Chia-Chin Wu ,Jack

指導教授：楊本立　　　　　Advisor：Ben-Li Young

國 立 交 通 大 學

電 子 物 理 系

碩 士 論 文

A Thesis

Submitted to Department of Electrophysics

College of Science

National Chiao Tung University

in partial Fulfillment of the Requirements

for the Degree of

Master

in

Electrophysics

July 2010

Hsinchu, Taiwan, Republic of China

中 華 民 國 九 十 九 年 七 月

含鐵超導材料 $FeSe_{1-\delta}$ 與銅摻雜之 $(Fe_{1-x}Cu_x)Se_{1-\delta}$ 的核磁共振研究

國立交通大學電子物理學系碩士班

學生：吳家慶　　　　　　　　　　　指導教授：楊本立 教授

中文摘要

　　我們利用固態核磁共振的方法研究最近發現的鐵基超導體 $FeSe_{1-\delta}$ 及摻雜銅元素取代部分鐵的 $(Fe_{1-x}Cu_x)Se_{1-\delta}$。這些樣品具有微量的 Se 缺陷($\delta \approx 0.12, 0.15$)。我們主要是探討 Se 缺陷和鐵元素在 $FeSe_{1-\delta}$ 中超導性所扮演的角色。由 Spin-lattice relaxation rate($1/T_1$)的實驗我們發現樣品中 spin fluctuation 的強度隨著 Se 缺陷的增加而變小，spin fluctuation 一般被懷疑與非傳統超導體有關，也確實出現在 $FeSe_{1-\delta}$ 的樣品中；另外分析 $1/T_1$ 數據發現並不是整體 $FeSe_{1-\delta}$ 樣品內部都具有超導性。藉由 AC susceptibility 實驗的量測，我們亦發現 $FeSe_{1-\delta}$ 在 Se 缺陷較多樣品中的 superconducting volume fraction 也較少。這些結果暗示著超導性只出現在 Se 缺陷較少甚至無 Se 缺陷的相中。。至於摻銅的 $(Fe_{1-x}Cu_x)Se_{1-\delta}$，我們的實驗發現摻銅效應導致超導臨界溫度下降且在極微量的銅摻雜($x \approx 0.03$)時 FeSe 的超導性消失，由我們的 $1/T_1$ 數據發現樣品的 Spin-lattice relaxation rate 在摻雜銅元素後並無明顯改變，表示摻雜銅元素對 $(Fe_{1-x}Cu_x)Se_{1-\delta}$ 內的 spin dynamic 影響不大 。對照 Williams 等人對摻雜銅 $(Fe_{1-x}Cu_x)Se_{1-\delta}$ 的電阻量測實驗發現有 metal-insulator phase transition，摻銅的效應對 FeSe 電子組態比 spin dynamic 的影響大，因此我們認為電子組態的變化可能是超導性消失的主因。

NMR study of Iron-based superconductor $FeSe_{1-\delta}$ and Cu-doped $(Fe_{1-x}Cu_x)Se_{1-\delta}$

Department of Electrophysics
National Chiao Tung University

Student: Chia-Chin Wu,Jack   Advisors: Ben-Li Young

Abstract

The roles of Se deficiency and Fe atoms, for the superconductivity of FeSe, have been respectively investigated in $FeSe_{1-\delta}$ and $(Fe_{1-x}Cu_x)Se_{1-\delta}$, by our NMR experiments. The data, for nuclear spin-lattice relaxation rate $(1/T1)$, show that the spin fluctuations are weakened at a larger δ, and are correlated with the superconductivity in FeSe. The superconducting volume fraction, estimated by our ac susceptibility experiments, is found to vary inversely with d. Our findings suggest that the Se-deficient FeSe has an inhomogeneous phase, where the superconductivity is associated with the regions having few or no Se vacancies. As for $(Fe_{1-x}Cu_x)Se_{1-\delta}$, T_c is rapidly suppressed by Cu doping and vanishes around x=0.03. The ^{77}Se and ^{63}Cu NMR linewidths suggest that a local moment is induced at the Fe sites, and not at the Cu sites. However, $1/T_1$ shows no obvious change with the Cu doping. We suspect that other effects, such as disorder or change in the density of states, have more influence on T_c suppression, since a metal-insulator transition, induced by Cu substitution, occurs in the resistivity measurements.

致謝

　　自從上了交大電子物理系，匆匆時光兩年已過，感謝母親的栽培，我才能有有機會考上交大電子物理所,在這段時間感謝楊老師對我的栽培與教導，也學到了核磁共振技術，雖然還是有許多不懂得地方，但對於物理中的複雜卻又有著如此巧妙的規律，讓我感受到物理的奧妙，這也是我當初會想考物理所的原因，之後即將要工作了，相信在電子物理系學到在研究物理時所必須具有的邏輯思考與大膽假設小心求證的思維，對我在思考事物有莫大的影響。

　　在就讀交大電物的期間，我認識了許多很棒的人，在韋儒身上學到了很多物理的知識，很多東西常常都要請教他，培源學長人很好，很照顧學弟，祝你的博士研究順利，也感謝宗佑給實驗室帶來的歡樂。另外在隔壁實驗室也認識許多朋友，學儒、耀宗、雅菁、佑廣、還有學弟妹們，不管在各方面，我在大家的身上也學了很多東西，也謝謝大家帶給我歡樂。中正的朋友們，常常跟大家一起吃飯打球聊天，謝謝大家陪我度過這段時光。還有宗穎，感謝你教我很多寫程式的知識，剛來交大的期間，也多虧有你的照顧，還有教會的朋友人都很好，是我見過最純真善良的人們。

　　在未來的日子裡，雖然大家都各奔前程，有的要從軍有的讀博班，也有要工作的，希望大家都會順順利利的，下次再遇到的時候，也許有的人都已經結婚生子，最後還是要感謝每一個我認識的人，沒有你們就不會有現在的我，謝謝。

Contents

Chapter 1 Introduction

1.1 Iron-based superconductors

The first member of iron-based superconductor LaFeOP, containing the Fe element, which was originally thought of against the formation of superconductivity, was first found by Hideo Hosono's research group at the Tokyo Institute of Technology in 2006[1]. Due to its low superconducting critical temperature, close to boiling point of liquid helium, LaFeOP, did not attract much attention. Until 2008, Hideo Hosono's research group found the second member of iron-based superconductor family, $La(O_{1-x}F_x)FeAs$, x=0.05~0.12[2]. This material has a relatively high superconducting critical temperature, T_c=26K. Then it has quickly drawn considerable attention. The emerge of iron-based superconductors did lead to a carnival-like atmosphere that scientists have tried synthesizing new members of iron-based superconductors and characterizing their properties.

After Japanese research group had successfully raised T_c up to 26K by replacing As with P, groups in china made similar compounds raised T_c to 56K. Although these T_c are not high enough to challenge the records set over the past twenty years by cuprate superconductors, scientists are still excited for several reasons. First, the critical temperature of Fe-based superconductors is much higher than conventional superconductors. Second, iron compounds have the potential for technological applications compared to copper oxides, which are too brittle to make wires for electric power transmission applications. Besides, superconducting iron is an unexpected element to make a superconductor because of magnetism is not compatible with superconductivity according to the conventional BCS theory. The Meissner effect also states that superconductors will expel magnetic fields. Why can the magnetism of the iron element coexist with the iron-based superconductors? There is no consensus on the answer yet.

There are four major kinds of Fe-based superconductors up to date. The first one is $La(O_{1-x}F_x)FeAs$, called the 1111 system. The second is $(Ba_{1-x}K_x)Fe_2As_2$ [3], called 122 system and having a higher T_c= 38K. The third is LiFeAs [4], belonging to the 111 system, and its T_c= 18K. The last is the $FeSe_{1-\delta}$ [5], belonging to 11 system and its T_c= 8K. Among the newly discovered iron-based superconductors, $FeSe_{1-\delta}$ is the first binary compound to be found by Dr. Maw-Kuen Wu's research group in the

Institute of Physics in Academia Sinica, Taiwan. Though its superconducting temperature is not as high as the other Fe-based superconductors, it has quickly attracted much attention due to its structural simplicity and easier material handling. Recently the high pressure experiments have raised its T_c up to 36.7 K [6], comparable to the FeAs-based superconductors.

Like the cuprate superconductors, some Fe-base superconductors need electron or hole doping in order to show superconductivity. For example, LaOFeAs is not superconducting, but $La(O_{1-x}F_x)FeAs$ is after F doping. By ultrafast laser experiment, pseudogap behavior is also found in some iron-based superconductors. Pseudogap behavior is considered as an important feature in cuprate superconductors.

1.2 $FeSe_{1-\delta}$ superconductor

FeSe resemble the FeAs-based superconductors in many ways. For example, both of them have layered structures, electronic states, and even the lattice instabilities [7-9]. However, whether FeSe is close to a spin-density wave (SDW) instability or magnetic order like the FeAs-based superconductors is still unclear[6,10].

$FeSe_{1-\delta}$ has complex structure phases, as summarized in the original literature where the superconductivity was reported in Se-deficient tetragonal β-FeSe[5], i.e., $FeSe_{0.82}$ and $FeSe_{0.88}$. And then it was soon followed by a similar finding for a composition of less Se deficiency, $FeSe_{0.92}$ [13]. However, recently McQueen's group claimed that superconductivity actually exists only in the nearly stoichiometric FeSe. They further pointed out that very little Se deficiency (δ=0.03) is enough to destroy the Cooper pairing in this material [14]. Although they attributed this discrepancy to the oxygen contamination in those Se-deficient FeSe samples, we would like to know why o $FeSe_{0.82}$ and $FeSe_{0.88}$ are still superconducting. Clarifying the role of Se deficiency in FeSe is essential to any theoretical treatments of pairing mechanism of superconductivity because it determines whether it is essential to introduce charge carriers in the two dimensional FeSe layer or not, as compared to the cuprate superconductors.

Understanding the role of Fe^{2+} spin is another important issue, which has already been investigated by chemically substituting Fe for Cu, i.e., $(Fe_{1-x}Cu_x)Se_{1-\delta}$[15,16]. Superconductivity in FeSe is rapidly suppressed by only 1.5% copper substitution. The iron (Fe^{2+}) ion and the copper (Cu^{2+}) ion have the same number of valence electrons but different spins and atomic radii. So the chemical

substitution is generally expected to alter the lattice and electronic structures, to introduce disorder and modify spin correlation. In this thesis, one of our works is also to check what causes suppression of superconductivity in the Cu-doped FeSe.

We have conducted the ^{77}Se NMR experiments and nuclear spin-lattice relaxation rates ($1/T_1$) on FeSe$_{0.88}$ and Cu-doped (Fe$_{1-x}$Cu$_x$)Se$_{1-\delta}$ in order to investigate the roles of Se deficiency and magnetic correlation in FeSe. Our results suggest that spin fluctuations are closely related to the superconductivity in FeSe, as the earlier study reported by Imai's group [11]. The nuclear spin-lattice relaxation rate ($1/T_1$) and superconducting volume fraction analyses in our study indicate that the Se-deficient FeSe has an inhomogeneous electronic state, where the cooper pairing mechanism occurs only in the regions with few or no Se vacancy, expanding upon similar results from previously reported NMR experiments [11,12]. This is supported by the decrease in spin fluctuation and superconducting volume fraction at larger Se deficiency.

As to Copper-doped FeSe, we have found that the NMR linewidth increases drastically upon Cu doping and then saturates rapidly. The reason that rapid suppression of superconducting critical temperature caused by copper-induced disorder correlated has also been investigated. In addition, we found that there is an interesting phenomenon that the spin-lattice relaxation rate ($1/T_1$) is nearly unchanged with copper-doping effect. So we suspect that the electronic band structure is altered more significantly than the spin dynamics because a metal-insulator transition was shown in the resistivity measurements [16]. This will be discussed later .
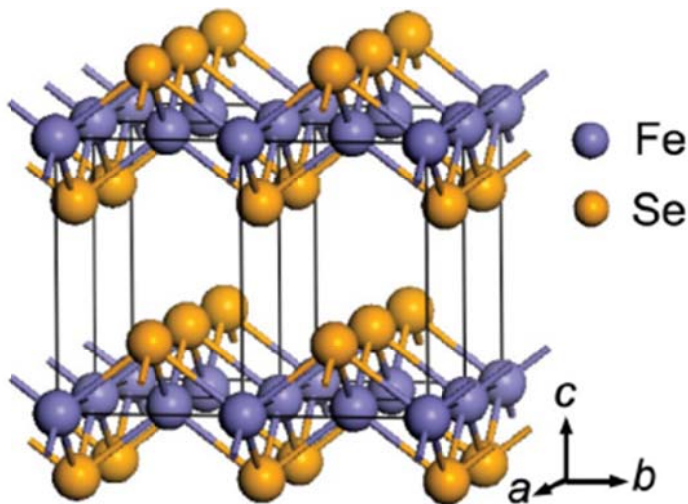

Figure 1-1. Schematic crystal structure (tetragonal)of _β-FeSe. Four unit cells are shown to reveal the layered structure. [5]

Chapter 2

Principles of nuclear magnetic resonance

2.1   Hamiltonian and spectra

The general form of nuclear spin Hamiltonian can be written as the sum of four interactions:

$$\mathcal{H} = \mathcal{H}_Z + \mathcal{H}_Q + \mathcal{H}_{e-n} + \mathcal{H}_{n-n},$$

The first term is the Zeeman Effect term of the nuclei, which can be written as:

$$\mathcal{H}_Z = \gamma \hbar \boldsymbol{H}_0 \cdot \hat{\boldsymbol{I}},$$

where γ is called gyromagnetic ratio. With this equation we can determine the desired NMR frequency we want to observe by changing the applied magnetic field, because the magnitude of energy between the energy levels is $\gamma \hbar \boldsymbol{H}_0 \cdot \hat{\boldsymbol{I}}$. If we apply a electromagnetic wave to the sample with some appropriate conditions, the nuclei will be excited to the higher energy level, where the frequency ω is exactly equal to $\gamma \boldsymbol{H}_0$. Figure 2-1 is an illustration of the energy levels of the 1/2 nuclear spin in the magnetic field. If we excite the nucleus in the ground state to the excited by applying a EM wave energy exactly equal to the energy gap between the two energy level, then the excited nucleus will return back to the ground state and emit photons, which gives on the NMR spectrum.
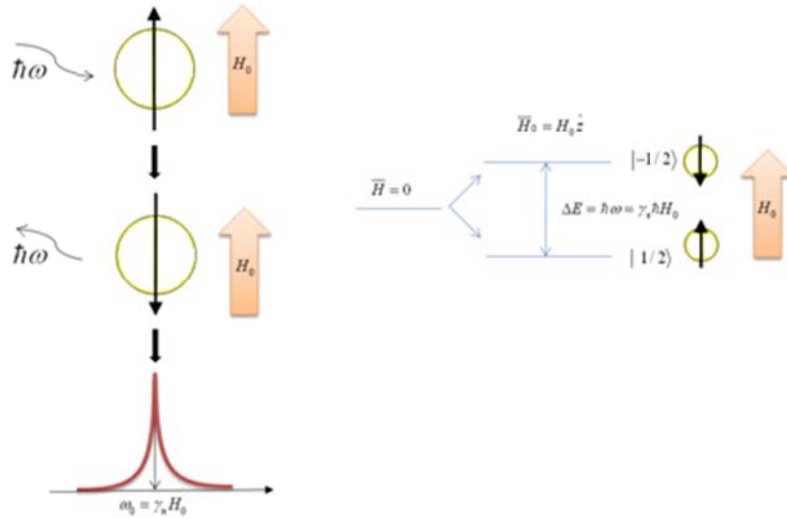
Figure 2-1. Illustration of spin 1/2 nucleus in magnetic field.

The third term is the interaction between e⁻ and nucleus, which can be written as:

$$\mathcal{H}_{e-n} = \mathcal{H}_F + \mathcal{H}_{dip} + \mathcal{H}_{orb} + \mathcal{H}_{trans}$$

This interaction is also called hyperfine interaction. $\mathcal{H}_F$ is call Fermi contact interaction, which happens between nucleus and S-wave election . $\mathcal{H}_{dip}$ is dipolar interaction, happening between nucleus and non S-wave election. $\mathcal{H}_{orb}$ is orbital interaction, happening between nucleus spin and orbital field. $\mathcal{H}_{trans}$ is called transferred interaction. It happens when the nucleus feels the magnetic field originated from outside, where the field is transferred by other conductive electrons. As for the remaining terms, $\mathcal{H}_Q$ and $\mathcal{H}_{n-n}$, are the quadrupolar interaction and dipolar interaction between nuclear spins, respectively, where the quadrupolar interaction occurs in the condition of the probing nuclear spin greater than 1/2 and with non-symmetric crystalline environment simultaneously. By the interaction of electric gradient and quadrupolar effect of nuclear spin, the NMR satellite lines will emerge. In another word, we can know the symmetry of the crystal structure of the sample by the NMR satellite frequency.

2.2 Bloch equations

The Bloch equations are listed below:

$$\frac{dM_z}{dt} = \gamma(\boldsymbol{M} \times \boldsymbol{H})_z + \frac{M_0 - M_z}{T_1},$$

$$\frac{dM_x}{dt} = \gamma(\boldsymbol{M} \times \boldsymbol{H})_x - \frac{M_x}{T_2},$$

$$\frac{\mathrm{d}M_y}{\mathrm{d}t} = \gamma(\boldsymbol{M} \times \boldsymbol{H})_y - \frac{M_y}{T_2},$$

The Bloch equation is a semi-classical way to describe the macroscopic magnetization which is the summation of the nuclear spins in condensed matter. By the semi-classical theory, we can know how to control the macroscopic magnetization. If we apply an appropriate radio frequency, technically called pulse in NMR, to the sample for the time we determine, then the total magnetization will be rotated to a designated orientation. With this we can easily have a physic picture of the NMR theory in condensed matter. The total magnetization alters with two time constants, T_1 and T_2, where the T_1 is spin-lattice relaxation time and T_2 is spin-spin relaxation time. T_1 corresponds to a longitudinal relaxation of the magnetization along the z-axis. T_2 corresponds to a transverse relaxation in the xy-plane. Figure 2-2 is an illustration for describing the dynamic process of the total magnetization of the nuclear spins. If we excite the sample by applying a right radio frequency, the nuclear spin system will enter a non-equilibrium state and return to the equilibrium state. The spending time depends on the spin-lattice relaxation time constant.
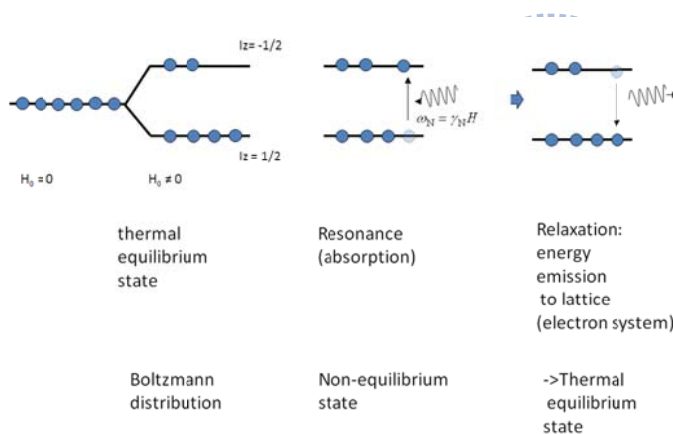

Figure 2-2. Spin-lattice relaxation process

2.3   Frequency shift and linewidth

The NMR frequency shift is a physical quantity to get the information of the local susceptibility in the sample. From the NMR spectra, we can know the position of the peak. By the equation of frequency shift, $\omega = \gamma(1 + K)H$, we will further get the local magnetic field information, from which we will know what interactions cause the shift. The interactions were already described in chapter 2.1. Through a NMR spectrum, we can obtain both the frequency shift and linewidth, where the shift reflects the local magnetization (or susceptibility) and the linewidth reflects the disorder in the material. Generally speaking, if the linewidth is bigger, the disorder in

the condensed matter is bigger.

2.4 Spin-lattice relaxation

The spin-lattice relaxation rate, $1/T_1$ can provide information of dynamic process, such as spin fluctuation. In order to explain T_1 briefly, we can introduce the Fermi golden rule, given by

$$P_{i \to f} = \frac{2\pi}{\hbar} |\langle i|\mathcal{H}_l|f\rangle|^2 \delta(\omega - E_f + E_i),$$

which represents the rate of transitions between two states. $\mathcal{H}_l$ is the time-dependent Hamiltonian giving rise to the spin-lattice relaxation. We can infer that the process of spin-lattice relaxation is related to the fluctuation of hyperfine field, so the $1/T_1$ can be written as:

$$T_1^{-1} = \frac{\gamma^2}{2} \int_0^\infty \langle \mathcal{H}_{hf}(t)\mathcal{H}_{hf}(0)\rangle e^{i\omega_0 t} dt,$$

where $\langle \mathcal{H}_{hf}(t)\mathcal{H}_{hf}(0)\rangle$ is the autocorrelation function. If the $\mathcal{H}_{hf}(t)$ alters between $\pm \mathcal{H}_{hf}$, then $\langle \mathcal{H}_{hf}(t)\mathcal{H}_{hf}(0)\rangle = \mathcal{H}_{hf}^2 e^{-t/\tau}$, where τ is the correlated time constant. Through further calculation, we can get

$$T_1^{-1} = \frac{\gamma^2 \mathcal{H}_{hf}^2 \tau}{1 + \omega_0^2 \tau^2}$$

With the above equation, we can know that if the electrons are becoming more correlated with neighboring electrons in strong correlated electron system, such as entering magnetic order or quantum critical point. The correlated time constant τ will become longer, which means the itinerant electrons in the material become more correlated through certain exchange interaction. Figure 2-3 is a simulated plot of $1/T_1$ versus $1/\omega\tau$. We consider there is a magnetic phase transition at T_m, where τ is temperature dependence. For a consideration of second order phase transition, $\tau(T)$ is given by,

$$\tau(T) = \tau_1(1 - T/T_m)^{\eta_1}, \text{ for } T<T_m$$
$$\tau(T) = \tau_2(T/T_m - 1)^{\eta_2}, \text{ for } T>T_m$$

In this picture, we can show that there is a peak of $1/T_1$, which occurs when the temperature is at T_m. From figure 2-3 we connect the spin-lattice relaxation with the physic picture of the electric correlation, which can explain the phenomenon of some critical phase transition, such as superconductivity, magnetic order, and et al. For further approaching to the classically representative plot of $1/T_1$ versus T, we plotted the $1/T_1$ versus T/T_m and found a singularity at T_m, which is in
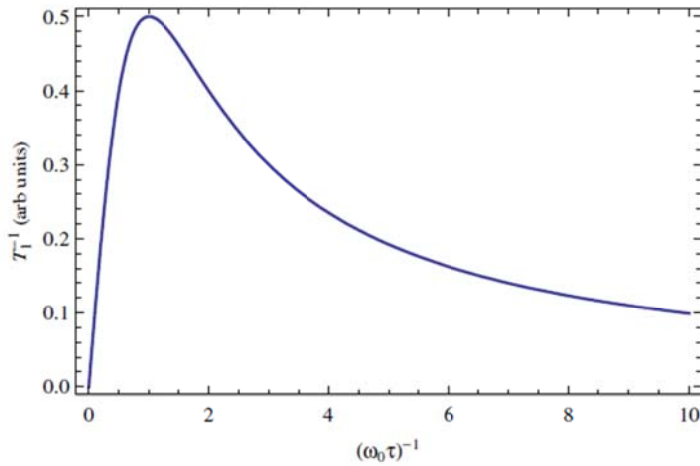
figure 2-4.

Figure 2-3. $1/T_1$ versus $1/\omega\tau$, where the peak is at phase transition temperature T_m.
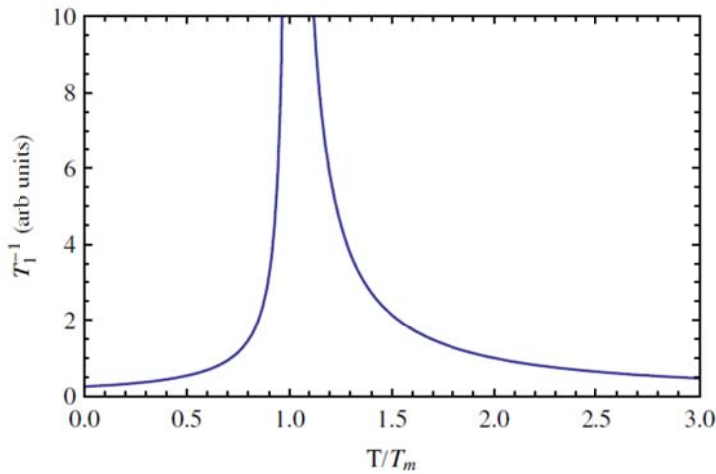

Figure 2-4. $1/T_1$ versus T/T_m.

For simple metal, we can use the Korringa relaxation, which is valid for non-interacting systems. It is given by

$$T_1 T K^2 = \pi^2 \hbar \gamma^2 / \mu_B^2$$

There is very few systems for which $\dfrac{T_1 T K^2}{K} = 1$, and we can measure the ratio of $\dfrac{T_1 T K^2}{K}$ to get the strength of quasiparticle interactions. In another form, Toru Moriya rewrited the $1/T_1$, which is given by

$$T_1^{-1} = \gamma^2 k_B T \lim_{\omega \to 0} \sum_{\mathbf{q}} A^2(\mathbf{q}) \frac{\chi''(\mathbf{q}, \gamma)}{\hbar\omega}$$

8

from which we can obtain the quantity of dynamic susceptibility. Usually the dynamic susceptibility is dominated by fluctuations, such as spin fluctuations in superconductivity. We can check that whether there are spin fluctuations in the high-T_c superconductors or other quantum critical phenomenon. Furthermore, we can write $1/T_1$ by employing the superconducting density of states, given by

$$T_1^{-1} \propto A^2 \int C_+(E, E') N_{BCS}(E) f(E) N_{BCS}(E') \times (1 - f(E')) dE$$

For a BCS superconductor, its density of state is given by

$$N_{BCS}(E) = \frac{E}{\sqrt{E^2 - \Delta^2}} N_N(E)$$

and the coherence factor is $C_+(E, E') = \frac{1}{2} + \frac{EE'}{2\Delta^2}$

At $E=\Delta$, N_{BCS} has a singularity and $C_+(E, E')$ is non-zero. Then the T_1^{-1} has a singularity at $T=T_c$. In a s-wave superconductor, $1/T_1$ has a maximum value, called Hibel-Slitcher coherence peak. For $T \leq T_c/3$, this equation can be reduced to $T_1^{-1} \sim \exp(-\Delta/k_B T)$. This behavior is only valid for s-wave. Different kinds of wave superconductor have different gap symmetry and we can get different power law relation of T_1^{-1} by introducing the density function.
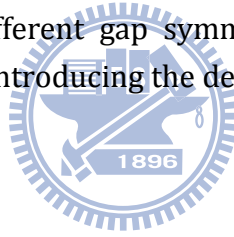
Chapter 3

NMR experimental methods and instruments

3.1   Fourier transformation in NMR

Ernst R. R. and Anderson W. A. first using the Fourier transformation technique in NMR experiment have greatly improved the sensitivity in NMR measurement. Generally, when we conduct the NMR measurement, we will also measurement the noise at the same time. Some of the noise is contributed by the amplifiers and other electronics in the spectrometer, but the major contributor is the thermal noise from the coil used to detect the signal. NMR is not a sensitive technique, so we have to take any ways we can to improve the signal-to-noise ratio in the spectrum. Nowadays, all the NMR experiments are F.T. NMR.

Figure 3-1 is an illustration of Fourier transformation in NMR. It is hard to observe the information in the FID time domain spectrum directly, so we need to transform the FID spectrum by Fourier transformation.
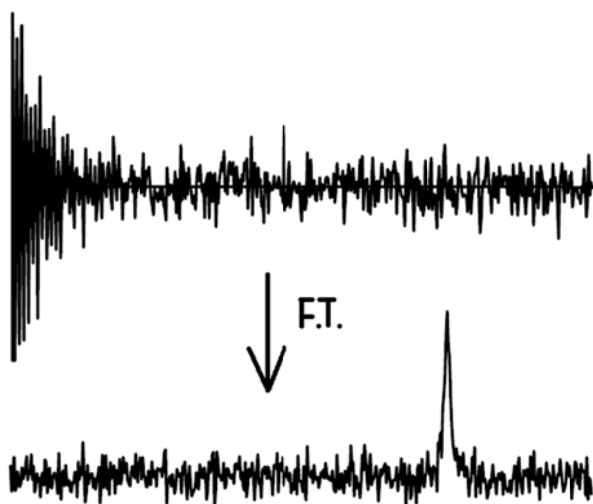

Figure 3-1. Illustration of Fourier transformation in NMR, which let us observe the frequency domain helping us justify the major frequency contribution of NMR spectrum directly.

3.2 Hahn spin echo

In 1950, Erwin Hahn burst on the world of science with his remarkable discovery or we can also say it's an invention, spin echo method [1]. The spin echo method provides an important way to the development of pulse methods in NMR, and therefore be ranked among the most significant contributions to magnetic resonance.

Hahn made the remarkable discovery that if we apply a second $\pi/2$ pulse a time τ after the initial pulse, miraculously there will appear another free induction signal at a time 2τ after the initial pulse. He named the signal the "spin echo". Figure 3-2 is a illustration of the sequence and the time evolution diagram of the spin echo. The physical basis of the spin echo method can be explained from the Bloch equations. One advantage of spin echo is that the inhomogeneity of the applied magnetic field causing a spread of spectrum can be gotten out.
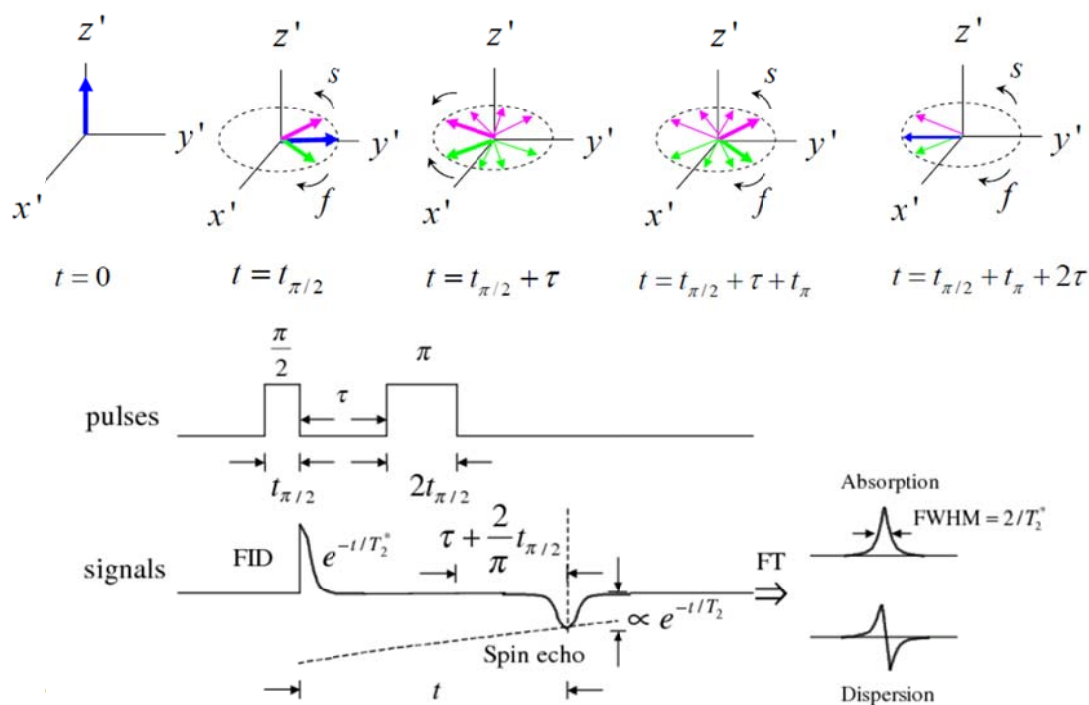

Figure 3-2. Illustration of the sequence and the time evolution diagram of the spin echo.

3.3 T_1 measurement (Inversion recovery method)

In order to get the information of the sample's spin-lattice relaxation time, the inversion recovery method was developed to get the T_1 data. All pulse NMR sequences for measuring the spin-lattice relaxation time T_1 either initialize the spin system and monitor its evolution or achieve a steady state condition in which the signal size depends on T_1. The former scheme involves a pulse (or a group of pulses) to prepare the nuclear spins in some non-equilibrium configuration and then, after some waiting period during which the spins are allowed to relax, a pulse monitors the state of the spins. The recovery of the nuclear spin population is monitored as a function of the waiting time. Figure 3-3 is a typical pulse sequence of the inversion recovery method. First we give a group of sequence, saturating the spin system, and then we wait a series of time. Third, we give a spin echo to detect the signal intensity. We will get a series of data as a function of time. Then we plot it as figure 3-4. The signal intensity of the spin system becomes stronger with the time. We fit the peaks and will get a magnetization curve (red dot line) as a function of time. The function of the curve is a exponential function, $M(t)=M(\infty)[1-\exp(-t/T_1)]$, where the T_1 is the spin-lattice relaxation.
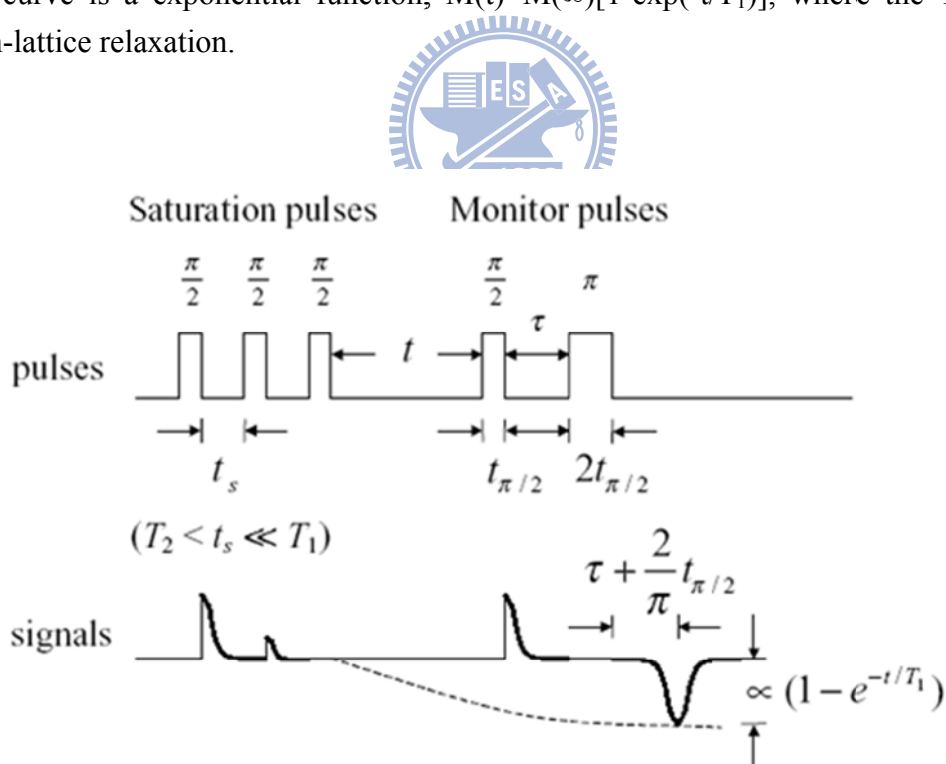

Figure 3-3. Pulse sequence of a T_1 measurement

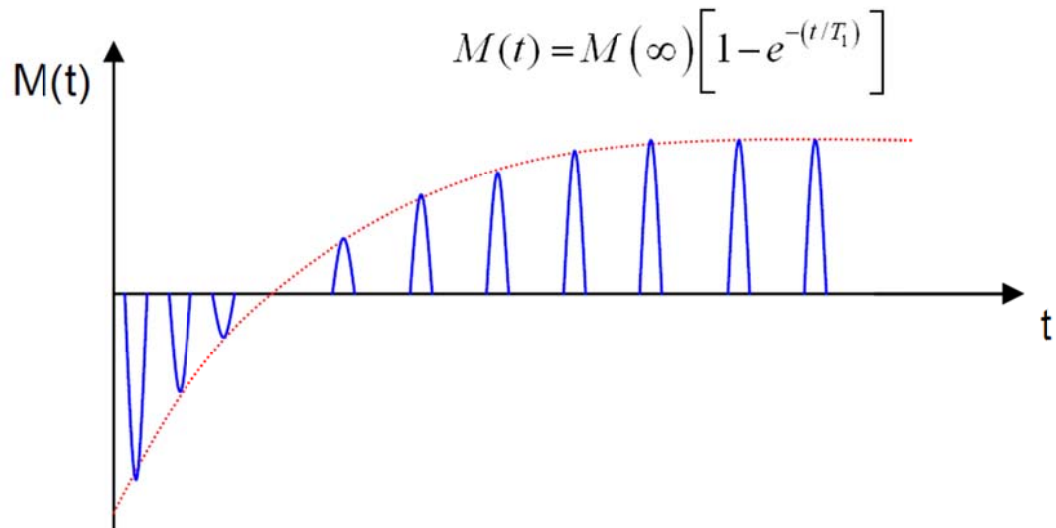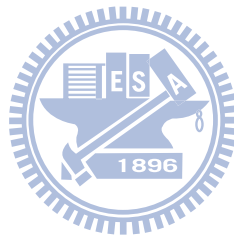$$M(t) = M(\infty)\left[1 - e^{-(t/T_1)}\right]$$

Figure 3-4. Magnetization intensity as a function

3.4 AC susceptibility measurement

The AC susceptibility experimental instrument is utilized our NMR probe circuits and the network analyzer. By measuring the resonance frequency of our LC circuit in the NMR probe, we obtain a rough data of susceptibility of sample. Figure 3-5 is a scheme of our AC susceptibility measurement. This data is a good tool to find whether there is a phase transition (superconductor, magnetic, structure) reflecting to their susceptibility. For example, if our sample enters antiferromagnetic order, the data will have a turning point, which tells us the Neel temperature of our sample. Besides, we can also determine the superconducting volume fraction by AC susceptibility measurement.
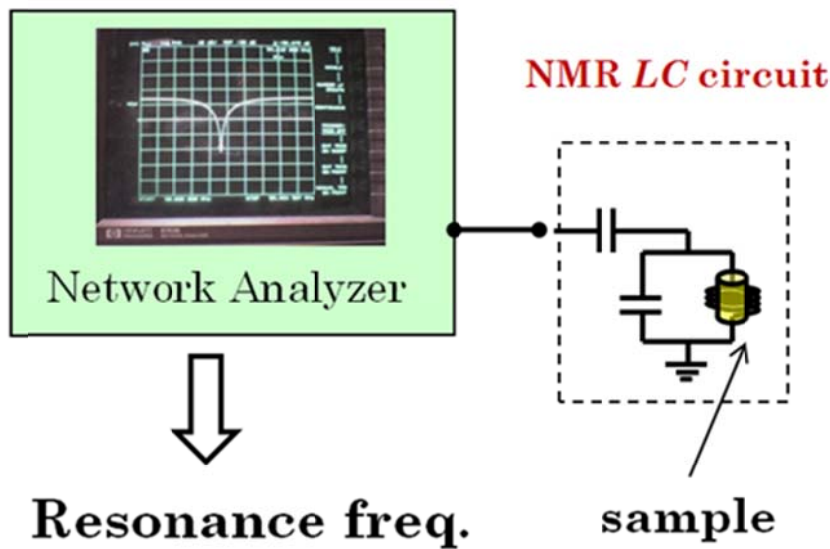
$$\omega(T) \sim \frac{1}{\sqrt{L(T)C}}, \qquad L(T) = L_0\left[1 + 4\pi\chi(T)\right]$$

Figure 3-5. Scheme of AC susceptibility measurement by NMR LC circuit.

3.5 Our instruments for NMR experiment

Our NMR system composes of a spectrometer, oscilloscope, magic T, superconducting magnet power supply, temperature controller, home-made probe, superconducting magnet Dewer, PC, pumping cooling system, and Helium recycling system. All the operations can be controlled automatically and remotely. We have a helium recycle system so that we can use the helium very efficiently.
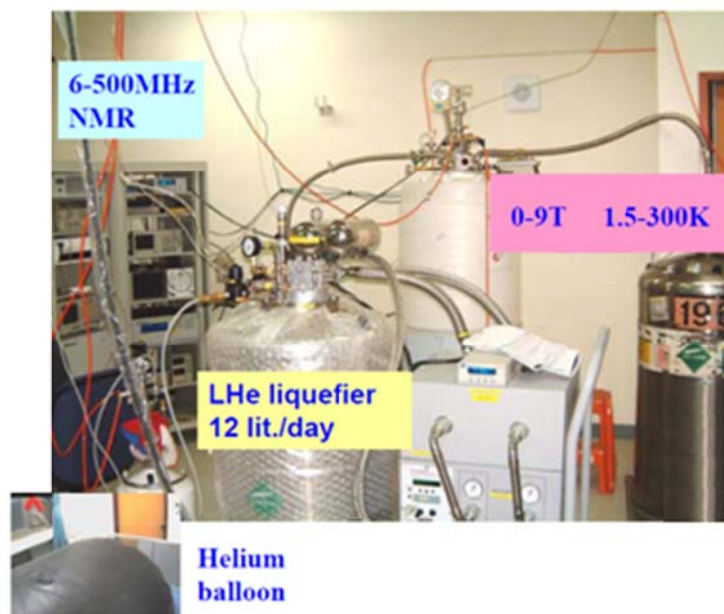

Figure 3-6. Picture of our NMR setup

Chapter 4 Experimental Process and Results

4.0 Brief description

Our experiments have several parts. The following experimental contents will be introduced in two parts based on the samples of Se-deficient $FeSe_{1-\delta}$ and Cu-doped $(Fe_{1-x}Cu_x)Se_{1-\delta}$, respectively. We have demonstrated our measurements of NMR, AC susceptibility, X-ray diffraction, and resistivity, where the NMR measurements include both of spectra and spin-lattice relaxation rate $(1/T_1)$.

4.1 Structure & Resistivity measurement & Phase diagram

Before the NMR measurement, we need to confirm that the Se-deficient $FeSe_{1-\delta}$ and Cu-doped $(Fe_{1-x}Cu_x)Se_{1-\delta}$ have the same tetragonal crystal phase where the superconductivity occurs. We also need to know the phase diagram of Se-deficient $FeSe_{1-\delta}$ in different Se deficiency and Cu-doped $(Fe_{1-x}Cu_x)Se_{1-\delta}$ in different doping level.

4.1.1 X-ray different patterns of $FeSe_{1-\delta}$ and $(Fe_{1-x}Cu_x)Se_{1-\delta}$

The samples of iron selenide (FeSe) are polycrystalline, provided by Maw-Kuen Wu's research group in the Institute of Physics in Academia Sinica, Taiwan. The detailed methods of sample preparation are in reference 1. Polycrystalline samples of the Se-deficient $FeSe_{0.88}$ and the Cu-substituted $(Fe_{1-x}Cu_x)Se_{1-\delta}$ with (x,δ)=(0,0.12), (0.01,0.15), (0.02,0.12), (0.03,0.12), and (0.04,0.12) were used in our NMR and ac magnetic-susceptibility experiments. In order to prove that the sample of $(Fe_{0.99}Cu_{0.01})Se_{0.85}$ has similar features with other samples, $(Fe_{0.98}Cu_{0.02})Se_{0.88}$, $(Fe_{0.97}Cu_{0.03})Se_{0.88}$, $(Fe_{0.96}Cu_{0.04})Se_{0.88}$, $FeSe_{0.88}$. Figure 4-1 is the powder x-ray diffraction patterns of these samples. Rietveld refinement was analyzed by using GSAS software, to confirm the sample stoichiometry and quality. The x-ray diffraction patterns reflect the detailed structures of our samples. Indeed, through the data on figure 4-1, the $(Fe_{0.99}Cu_{0.01})Se_{0.85}$ does have similar structure with other different composition of samples.
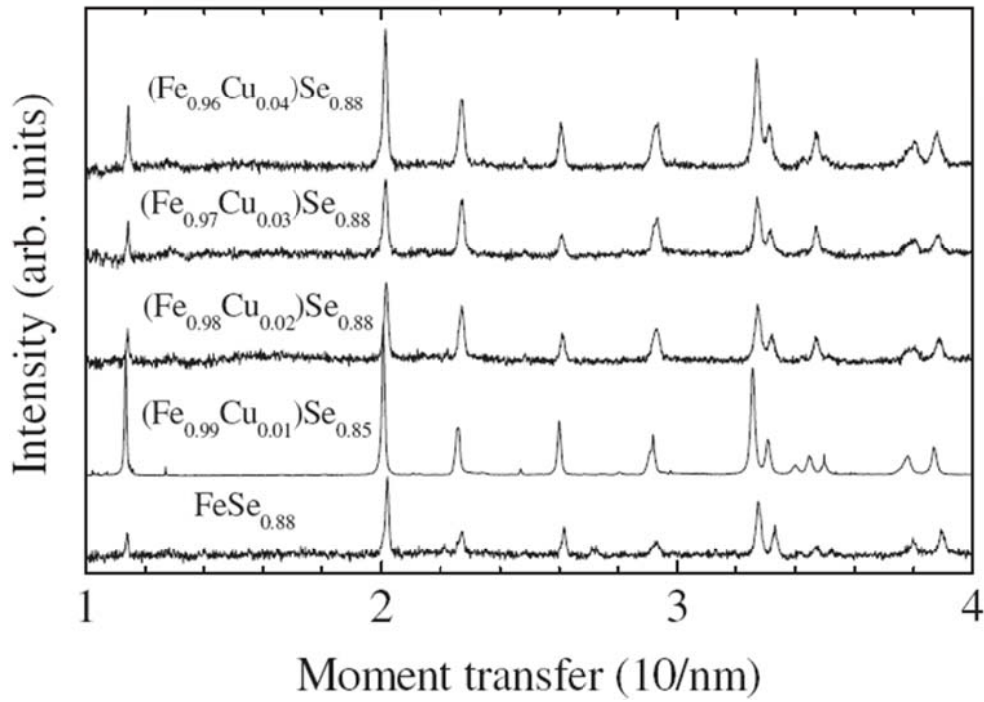
Figure 4-1. Powder x-ray diffraction patterns of $(Fe_{0.99}Cu_{0.01})Se_{0.85}$, $(Fe_{0.98}Cu_{0.02})Se_{0.88}$, $(Fe_{0.97}Cu_{0.03})Se_{0.88}$, $(Fe_{0.96}Cu_{0.04})Se_{0.88}$, $FeSe_{0.8}$. The horizontal axis is the moment transfer, $M = 4\pi \sin(\theta)/\lambda$.

4.1.2 Resistivity measurements of FeSe$_{1-\delta}$ and (Fe$_{1-x}$Cu$_x$)Se$_{1-\delta}$

Figure 4-2 is the resistivity (normalized to 300K) of different Cu contents of (Fe$_{1-x}$Cu$_x$)Se$_{1-\delta}$. Note that a metal-insulator transition is observed in both of our samples and A. J. Williams's research group [2,3]. From figure 4-2, very few Cu doping level as an amount of 0.01 have changed superconducting critical temperature (~5K). By the way, we noted that Cu doping concentration at 0.03 is enough to destroy the superconductivity in (Fe$_{1-x}$Cu$_x$)Se$_{1-\delta}$. For more Cu doping concentration greater than 0.03, resistivity is becoming bigger, which may be thought as a metal-insulator transition.

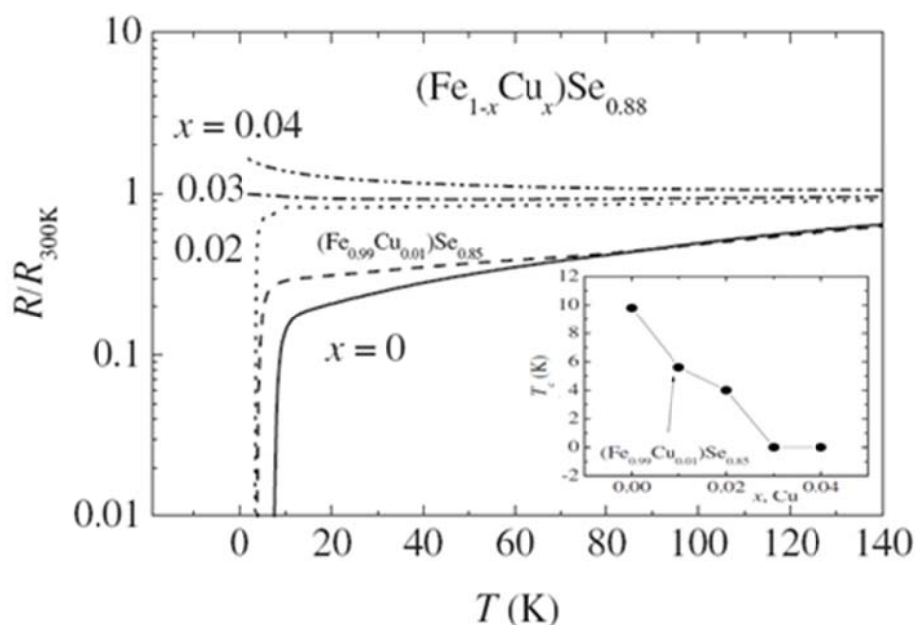**Figure 4-2.** Resistivity (R) data for different copper content of (Fe$_{1-x}$Cu$_x$)Se$_{1-\delta}$ samples, where there is selenium content of 0.85's sample proved having similar structure with other samples. All data has been normalized to room temperature values (R$_{300K}$). Inset shows the T$_c$ with different doping level.

4.1.3 Phase diagram of FeSe$_{1-\delta}$

Figure 4-3 gives the T_c onset to the different Se deficiency of the FeSe$_{1-\delta}$. If we ignore the FeSe$_{0.97}$ case, we can find that the structural disorder has little effect on T_c. The FeSe$_{0.97}$ anomaly is due to the method of sample preparation, which Imai et al. added a quench processing to the preparing method and caused an instability of structure order, an undesired hexagonal structure phase (superconductivity exists in tetragonal phase).
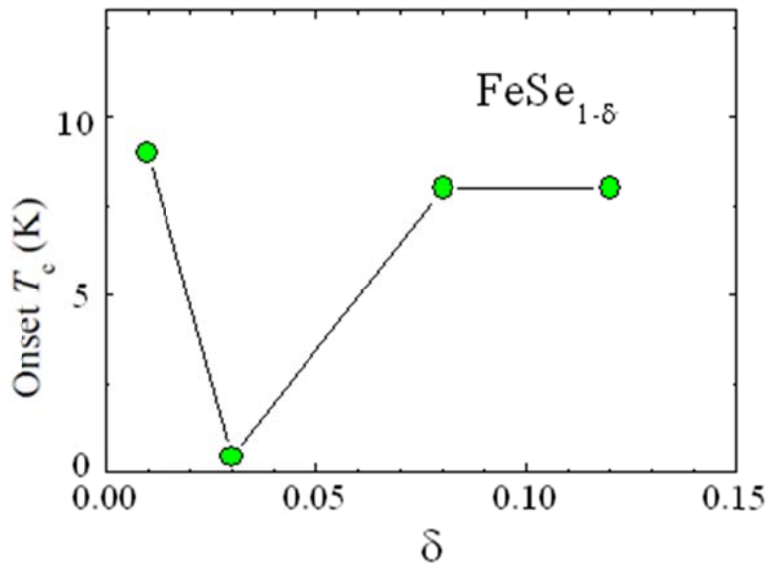
Figure 4-3. T_c onset for different Se-deficient FeSe$_{1-\delta}$. Besides the FeSe$_{0.97}$ case, the Structural disorder has little effect on T_c.

4.1.4 Phase diagram of $(Fe_{1-x}Cu_x)Se_{1-\delta}$ with different Cu doping level

Figure 4-4 shows the phase diagram of $(Fe_{1-x}Cu_x)Se_{1-\delta}$ with different Cu doping level. We see that the superconducting critical temperature T_c was suddenly suppressed by very few Cu doping concentration of 0.03, and then the superconductivity vanished.

Figure 4-4. T_c onset for different Cu doping level

4.2   AC susceptibility measurements of $FeSe_{1-\delta}$ and $(Fe_{1-x}Cu_x)Se_{1-\delta}$

Experimental setup is described in chapter 3-4(p.14)

4.2.1 Theory of AC susceptibility measurements

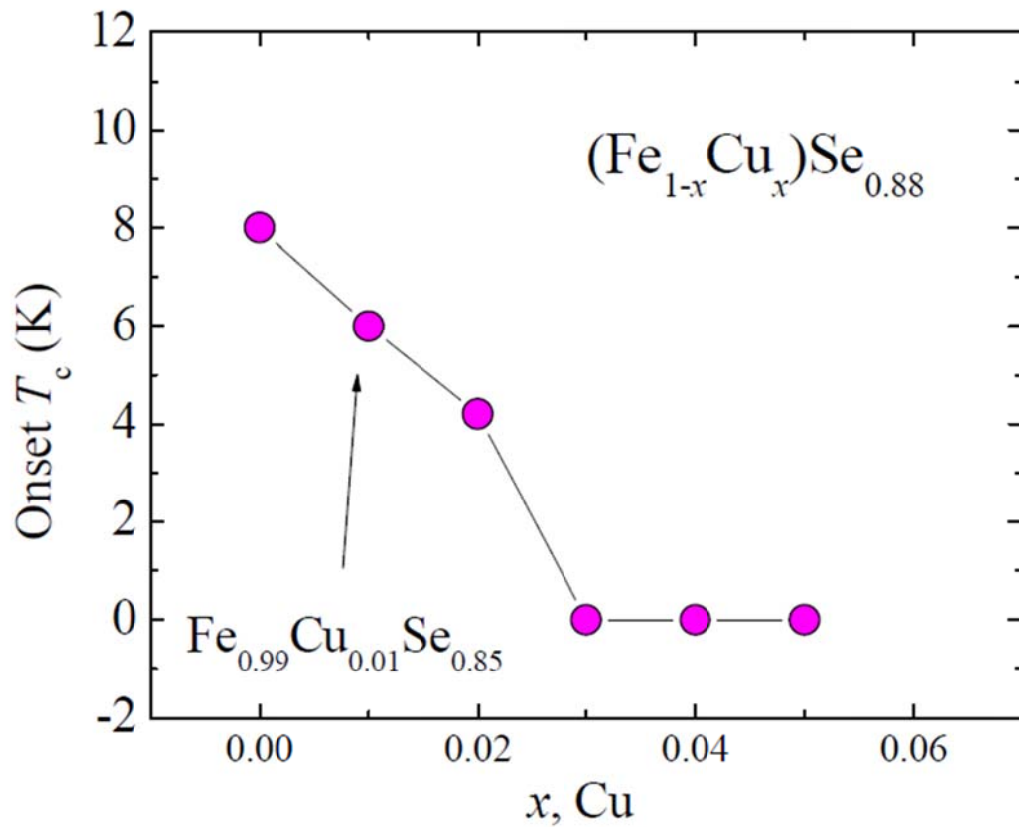We want to know why $FeSe_{0.99}$, $FeSe_{0.92}$, $FeSe_{0.88}$ have similar onset T_c? The superconducting volume fraction estimated from our ac susceptibility may provide a clue. Figure 4-5 shows our ac susceptibility measurements of Imai et al.'s $FeSe_{0.99}$, our $FeSe_{0.88}$, $(Fe_{0.99}Cu_{0.01})Se_{0.85}$, and $(Fe_{0.98}Cu_{0.02})Se_{0.88}$. The method of measurement is using the LC resonant circuit, originally made for NMR's measurements, to detect its relative frequency shift by using the Network analyzer [4]. This method utilizes the resonance frequency ω ($\sim 1/\sqrt{LC}$) of the LC circuit changing with the inductance, which in turn depends on the sample susceptibility χ. That is, $L=L_0[1+4\pi\chi(T)]$, L_0: inductance of the NMR coil. The rising of the frequency-shift ratio [defined as relative size of change from the frequency at 15K, $\omega(T)/\omega(15K)-1$] in figure 4-5 represents the superconducting phase transition because the frequency ω increases as it enters the superconducting state, $\chi<0$. The size of frequency-shift ratio gives a rough estimate of the superconducting volume fraction.

4.2.2 Superconducting volume fraction of $FeSe_{1-\delta}$ & $(Fe_{1-x}Cu_x)Se_{1-\delta}$

We found that $FeSe_{0.88}$ has a superconducting volume fraction significantly smaller than $FeSe_{0.99}$ since a small frequency-shift ratio. The dc bulk susceptibilities, reported in reference 12, show the similar result of a weaker superconducting diamagnetic response in $FeSe_{0.82}$, if the background sign from impurities is subtracted. Note that the pressure experiment on $FeSe_{0.99}$ shows that T_c and superconducting volume fraction vary simultaneously with pressure [4], unlike in the Se-deficient case, where only superconducting volume fraction varies with Se deficiency. We also did the two-T_1 analysis for our $FeSe_{0.88}$ and found that the volume fraction, for the short T_1 component, is about 50%, which is 10% less than that in $FeSe_{0.92}$ [6].
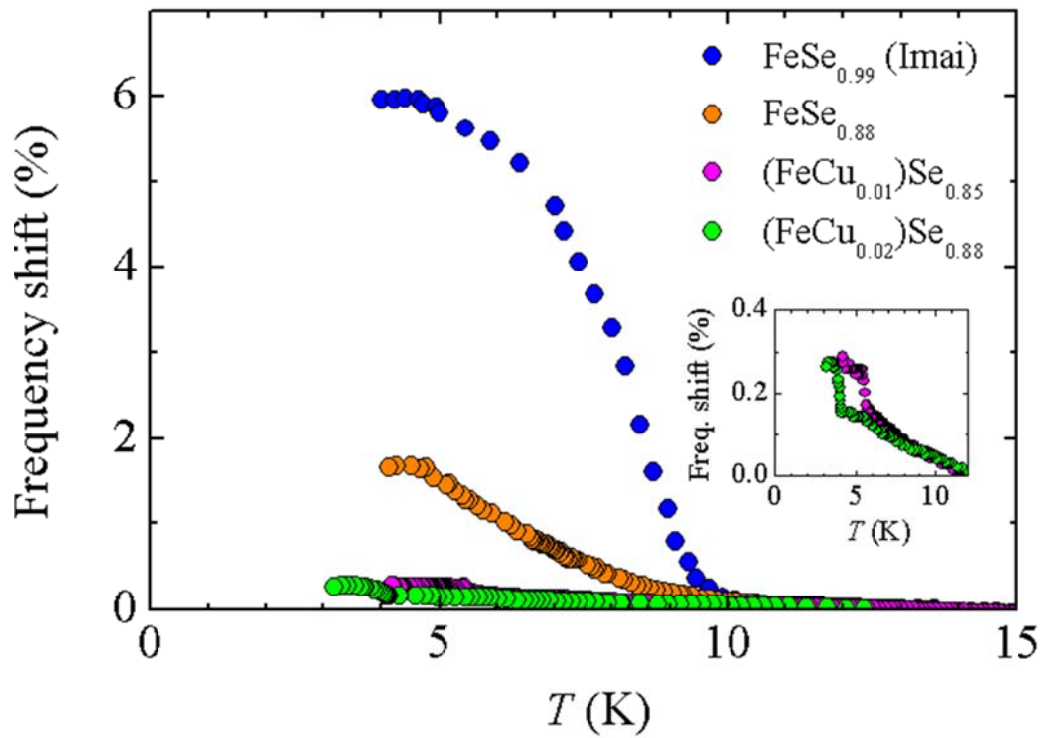
Figure 4-5. Data from the AC magnetic susceptibility measurements of $FeSe_{0.99}$ (reproduced from reference 7), $FeSe_{0.88}$, $(Fe_{0.99}Cu_{0.01})Se_{0.85}$, and $(Fe_{0.98}Cu_{0.02})Se_{0.88}$. The frequency shift, on the vertical axis, is defined as relative size of change from the frequency at 15K, $\omega(T)/\omega(15K)-1$.

4.3 NMR spectrum of FeSe$_{1-\delta}$

To our knowledge, there are three papers of NMR measurements, to date, reporting on superconductivity in FeSe$_{1-\delta}$. Imai's research group has measured the nearly stoichiometric FeSe$_{0.99}$ and FeSe$_{0.97}$, with the samples claimed to be free of oxygen contamination [4]. Kotegawa's research group and Masaki's research group have also measured the Se-deficient FeSe$_{0.92}$ but didn't say whether there was any oxygen contamination or not [5,6]. In order to resolve this discrepancy, concerning the stoichiometry of the superconductivity in FeSe, the following discussions compare to our FeSe$_{0.88}$ data, with the data reproduced from the previous literature. The standard Hahn-echo pulse sequences and saturation pulses were, respectively, employed throughout our ^{77}Se NMR spectra and $1/T_1$ experiments at 75 kilo Gauss (kG).

4.3.1 NMR spectrum of FeSe$_{1-\delta}$

Figure 4-6a is the ^{77}Se NMR spectra with different Se deficiency of FeSe$_{1-\delta}$, FeSe$_{0.99}$, FeSe$_{0.97}$, FeSe$_{0.92}$, FeSe$_{0.88}$, at 10 K. Note that the linewidth increases with the Se deficiency, as expected because NMR linewidth generally reflects the amount of lattice disorder in the sample. From the spectra of different Se deficiency of FeSe$_{1-\delta}$, we can indirectly confirm the correct stoichiometry of these samples. We compare the spectra of disordered FeSe$_{0.88}$ and ordered FeSe$_{0.99}$. Similar $T_c \approx 8K$ suggests that Cooper pairing is not vulnerable to the lattice disorder induced by the Se vacancy.

How can we be sure that the growing linewidth reflects the lattice structure disorder caused by Se vacancy? Figure 4-6b is a simulating diagram which is assumed that we consider different quantity of vacancy in a condensed matter. If the vacancy is bigger, then the linewidth is getting bigger, too. Notice that the frequency shift behavior is not so clear in our experimental data. We thought it is because of the experimental error problem.

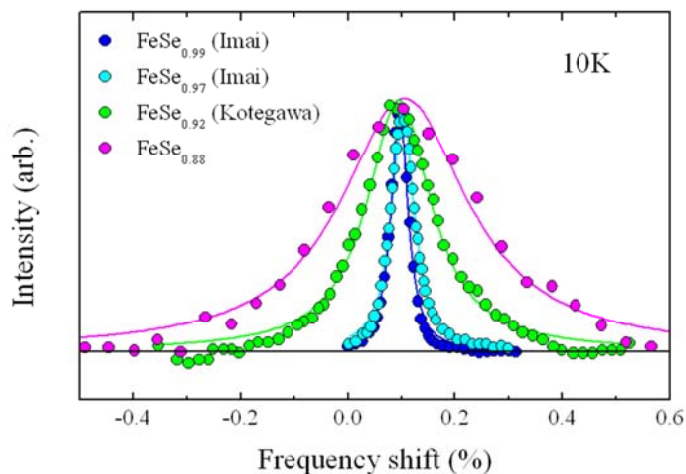**Figure 4-6a.** ^{77}Se NMR spectra, at 10K, for different Se-deficient FeSe$_{1-\delta}$. Data for FeSe$_{0.97\&0.99}$ and FeSe$_{0.92}$ are reproduced form references 7 and 13, respectively.
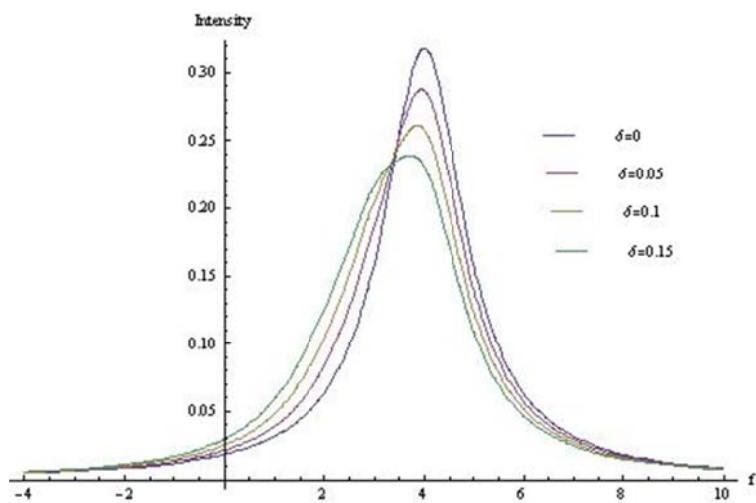

Figure 4-6b. Simulating diagram assumed by structure disorder behavior

4.3.2 Linewidth and frequency shift from NMR spectrum of $FeSe_{1-\delta}$

Figure 4-7 is the frequency shift and spread of shift to the Se deficiency from the NMR data of $FeSe_{1-\delta}$ in figure 4-6. We note that the frequency shift (K) doesn't change much with the Se deficiency (δ), which means that the "local" spin susceptibility χ does not change much either because frequency shift is proportional to the spin susceptibility ($K \propto \chi$). Note the local word with quotation marks because NMR is a technique utilizing the nuclei as a local probe to detect the environment of the material. The results of local susceptibilities with different Se deficiency differ from the results of bulk susceptibility measurement, done by Williams's research group [3], where the bulk susceptibility increases significantly with Se deficiency (δ). We attribute this discrepancy to the impurity phases from excess iron or iron oxides resulting from the oxygen contaminations. We didn't observe magnetic broadening of the linewidth at low temperature of our temperature-linewidth data, so we think there was no or few magnetic impurities bonded to the FeSe samples. The linewidth for our $FeSe_{0.88}$ is nearly temperature independent, from 70K down to T_c, as was the case for $FeSe_{0.92}$ in reference 5. Therefore, based on NMR frequency shift and linewidth data, there are no impurity phases entering the $FeSe_{1-\delta}$ with different Se deficiency, but we cannot exclude the possibility of oxygen contamination in $FeSe_{1-\delta}$ for $FeSe_{1-\delta}O_y$, indicated by McQueen's group [7]. We will leave this to later discussion.
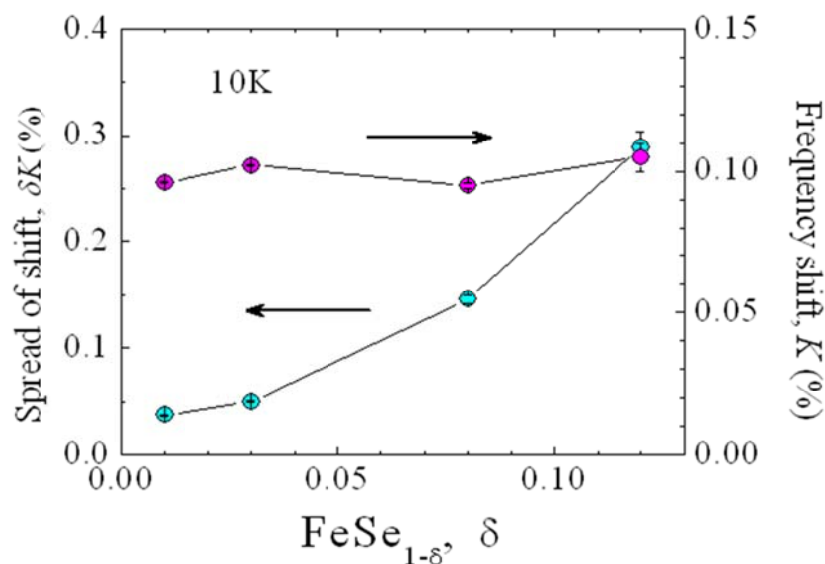

Figure 4-7. Frequency shift and the spread of shift, derived from the spectra on figure 4-6.

4.4 Spin-lattice relaxation rate ($1/T_1$) of $FeSe_{1-\delta}$

Here we report our spin-lattice relaxation data of $FeSe_{1-\delta}$ and discuss what we have found in our sample. First, I will present a representative $1/T_1$ data of $FeSe_{0.88}$ (at 16K) and explain why we use a stretched exponential curve fitting. Second, we discuss the behavior of the distributed T_1 in our sample.

4.4.1 Spin lattice relaxation curve of $FeSe_{0.88}$

Figure 4-8 represents a nuclear spin-lattice relaxation curve for our $FeSe_{0.88}$ sample at 16K. Note that M(t) means the nuclear magnetization as a function of time. The function of typical single exponent spin lattice relaxation curve is given by,

$$1 - \frac{M(t)}{M(\infty)} = e^{-\frac{t}{T_1}}$$

Note that the dashed line in the log plot of figure 4-8. It means if the curve is single exponential, the curve will be a straight line following the trace of dashed line. If the curve deviate the dashed line, it can't be classified into the type of single exponential curve, which means the curve is follow a single exponential behavior. So we should fit the curve with another kind of curve fitting, such as the following stretched exponential curve fitting.

Compare our $FeSe_{0.88}$ data with the Imai's group's $FeSe_{0.99}$ and $FeSe_{0.97}$ data, there were two different behaviors. For the Imai's group's $FeSe_{0.99}$ and $FeSe_{0.97}$ data, is single exponential, as to ours, $FeSe_{0.88}$, is stretched exponential. The observed stretched exponential behavior means that the spin-lattice relaxation rate, T_1, is distributed in our $FeSe_{0.88}$ sample. This behavior may be caused by two reasons, anisotropy or disorder in $FeSe_{0.88}$. To figure out what the real reason causing distributed behavior in $FeSe_{0.88}$, we note that the single exponential behavior, observed in the nearly stoichiometric FeSe polycrystalline samples, implies that there is only a nearly isotropic T_1, although it has a two-dimensional layered structure. So a stretched exponential behavior, caused by the anisotropic T_1, is then ruled out. So the reason causing distributed behavior in $FeSe_{0.88}$ is due to the disorder induced by Se-vacancy.
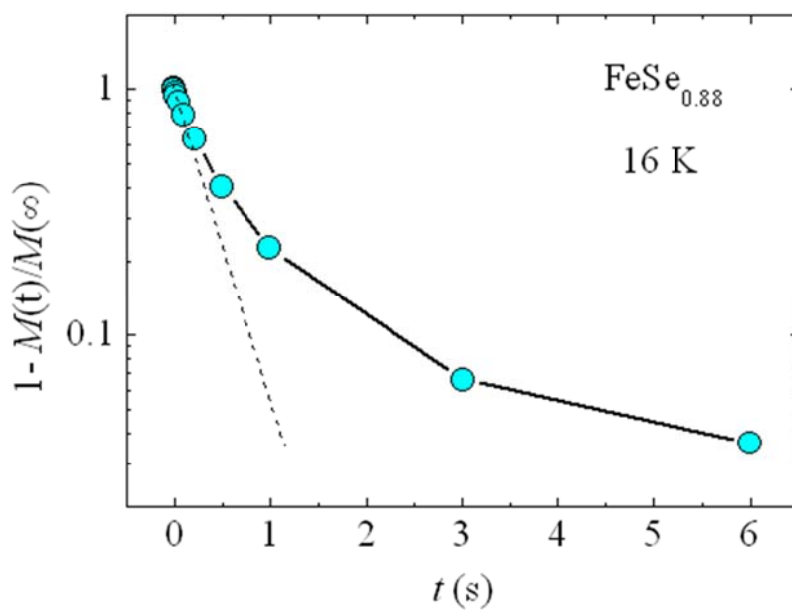
Figure 4-8. [77]Se nuclear spin-lattice relaxation curve for FeSe$_{0.88}$ at 16K [M(t):nuclear magnetization]. Dashed line is the single exponential curve.

4.4.2 Behavior of distributed $T_1(T)$ in $FeSe_{0.88}$

Figure 4-9 is the stretched exponent (α) obtained from a stretched exponential curve fitting. From figure 4-9, we observed a temperature-dependent exponent behavior implying that the different Se sites have the different temperature-dependent spin-lattice relaxation rate ($1/T_1$). We find that all the Se nuclear sites have similar spin-lattice relaxation rate at high temperature, whereas there is distributed spin-lattice relaxation rate ($1/T_1$) at low temperature, where the stretched exponent α is close to 0.6. Similar behavior was also reported by Kotegawa's research group, for $FeSe_{0.92}$ [5]. To summary, we found that there are different temperature dependent T_1 due to the disorder induced by Se vacancy in $FeSe_{1-\delta}$.
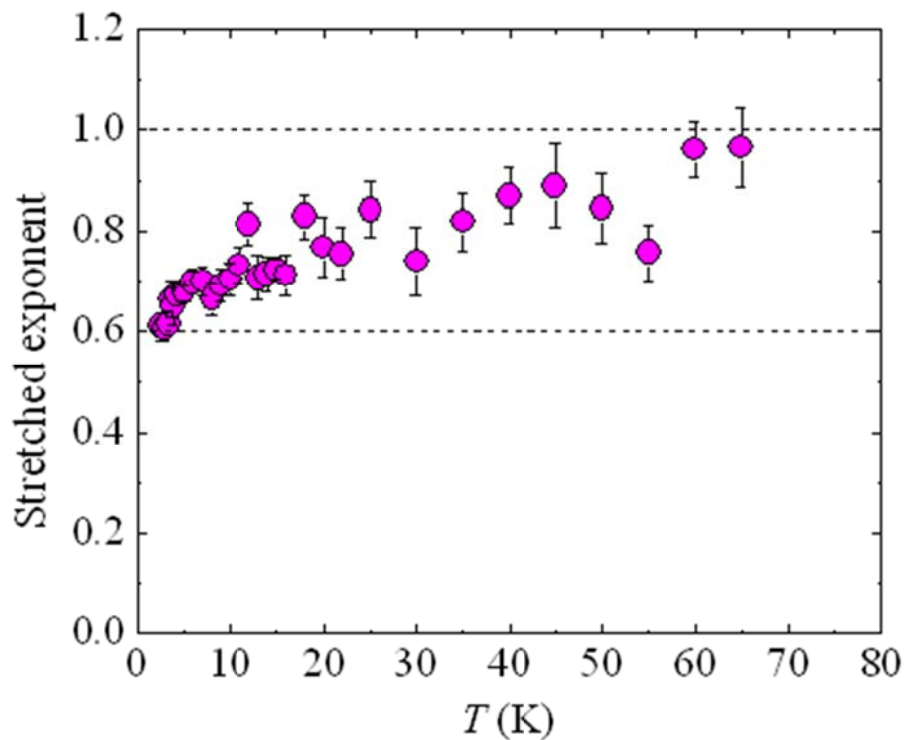

Figure 4-9. Stretched exponent from the stretched exponential curve fitting [$e^{-(t/T_1)^{\alpha}}$]. Note that different Se sites have different temperature-dependent T_1.

4.4.3 $1/T_1T$ in FeSe$_{1-\delta}$ with different Se deficiency

Figure 4-10 shows the relaxation rate curve, with different Se deficiency, from the stretched fit. Note that T_1 value is not directly obtained from the stretched exponential curve fitting. The T_1 value of the stretched exponential curve fitting is the most majority of T_1 in the sample. In order to catch the intrinsic feature from the distributed T_1, we calculated the average $1/T_1$, directly from the initial slope of the relaxation curve[8], instead of two-T_1 fit. The equation of average $1/T_1$ in stretched exponent curve fitting is given by

$$\langle\frac{1}{T_1}\rangle = \int_0^\infty \frac{1}{T_1} P\left(\frac{1}{T_1}\right) d\left(\frac{1}{T_1}\right) = \ln 10 \times \text{initial slope of } \log(1 - \frac{M(t)}{M(\infty)})$$

The pink circles are our $1/T_1T$ curve. From this curve, we saw the turning point reflecting the T_c. The Korringa-type behavior (T_1T=constant), for temperatures between superconducting temperature (T_c) and 50 K, in FeSe$_{0.88}$ and FeSe$_{0.92}$, is actually misleading because both $1/T_1$ values of FeSe$_{0.88}$ and FeSe$_{0.92}$ are obtained from the stretched exponential fit. These stretched data cannot reflect the real situation of the average behavior for $1/(T_1T)$ because the stretched exponent is proved to be temperature dependent (see figure 4-9). Above 100 K, T_1 is uniquely determined, and $1/(T_1T)$ increases with increasing temperature. The behavior is common to some Fe-Based superconductors, and likely originated from the effect of the band structure in electron-doped system. The increasing $1/(T_1T)$ with increasing temperature above 100K may be caused by pseudogap behavior in electron-doped system of Fe-Based superconductors.

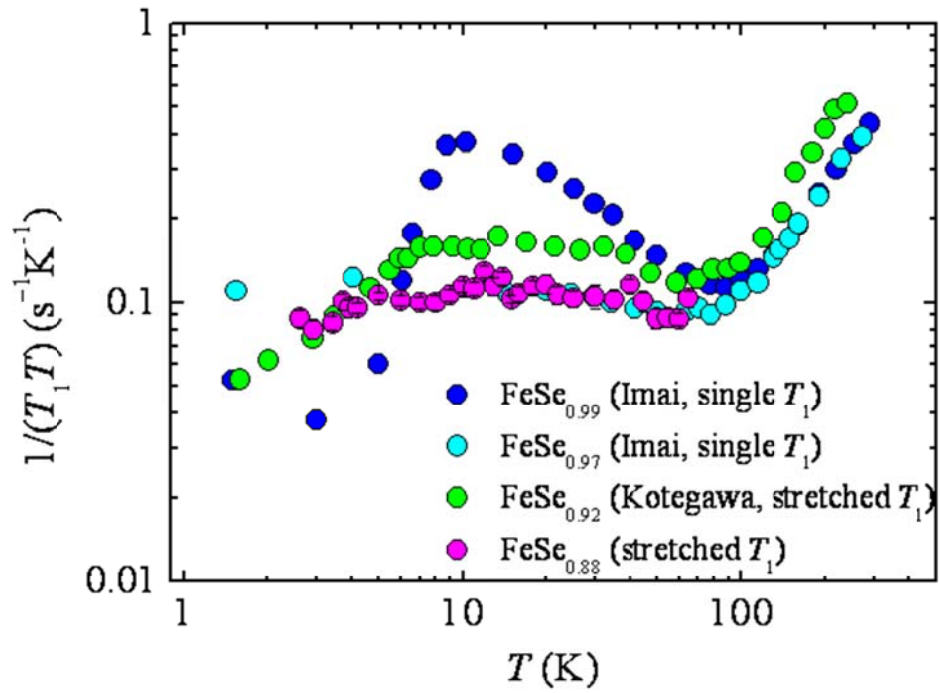**Figure 4-10.** Plot of ^{77}Se $1/(T_1T)$ as a function of temperature. Data for FeSe$_{0.99}$ and FeSe$_{0.97}$ are single-T$_1$, where $1/(T_1T_c)$ decreases with δ. The picture reflects the magnetic fluctuations in different Se-deficient FeSe$_{1-δ}$.

4.4.4 $1/T_1T$ by two-T_1 curve fitting of FeSe$_{0.88}$ & FeSe$_{0.92}$

Compare with the stretched eponential fitting, Masaki et al. have fit their FeSe$_{0.92}$ relaxation curves, using two-T_1 function, and found that the short T_1 component displays an enhanced $1/T_1$ similar to the nearly stoichiometric FeSe$_{0.99}$ [6]. The upward $1/(T_1T)$, just above T_c, has been considerd as evidence for the connection of spin fluctuations to superconductivity in FeSe [4]. We also used the two T_1 method for fittng our T_1 data. Figure 4-11b is our plotting of $1/(T_1T)$ of FeSe$_{0.88}$. Figure 4-11c is Masaki et al.'s plotting of $1/(T_1T)$ of FeSe$_{0.92}$, fit by two-T_1 and stretched exponential functions, respectively. The function of two T_1 fitting is given by

$$M(t) \propto Ae^{-\frac{t}{T_{1,short}}} + (1-A)e^{-\frac{t}{T_{1,long}}}$$

From the two-T_1 fitting we obtained the volume fraction parameter of short $T_1(A)$, where our volume fraction A is 0.5 for FeSe$_{0.88}$ and Masaki et al.'s is 0.6 for FeSe$_{0.92}$. The short T_1 is considered as the contributor to the superconductivity. This is a good agreement with that the level of Se deficiency is proportional to disorder and superconducting volume fraction in FeSe$_{1-\delta}$, obtained from our AC susceptibility measurements.

There is a problem with the two-T_1 fitting. In Masaki et al's plotting, the long T_1 curve originally thought of non-superconducting part still has a turning point of superconductivity. So the two-T_1 is not a good fitting method for the FeSe$_{1-\delta}$, although the long T_1 curve of our plotting seems having no turning point of superconductivity. One possible reason is that maybe there are both two kinds of superconducting electrons, conventional and unconventional, in FeSe. So in low temperature, long T_1 curve still has a turning point caused by the conventional superconducting electrons
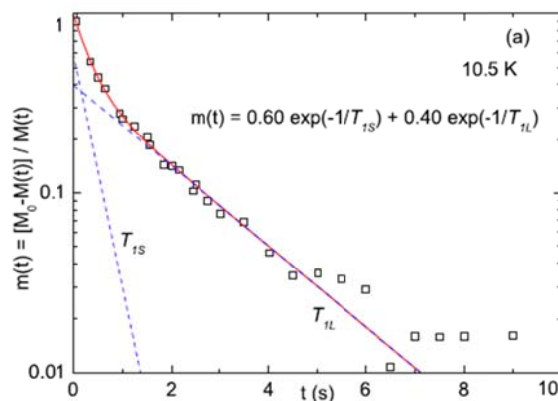

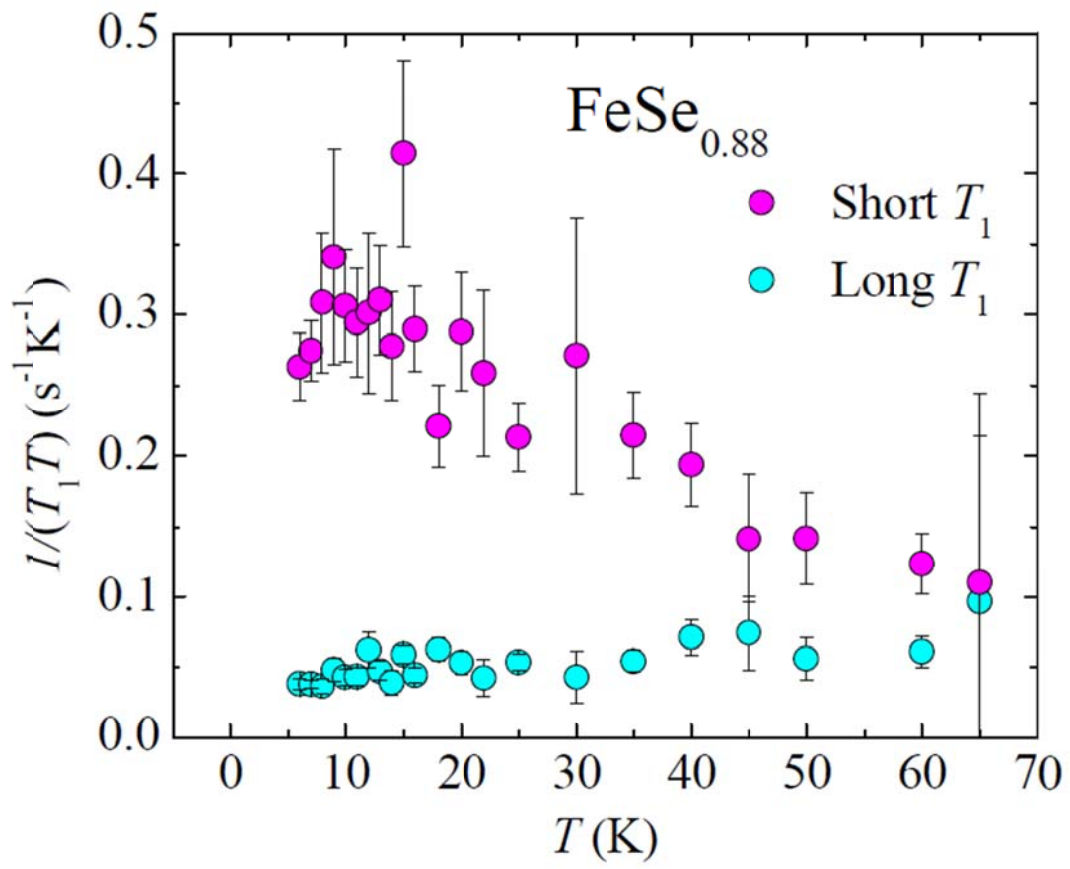**Figure 4-11a.** Fitting lines of two components method.(Masaki et al.)[6]

Figure 4-11a. We used two-T_1 fitting for our FeSe$_{0.88}$.
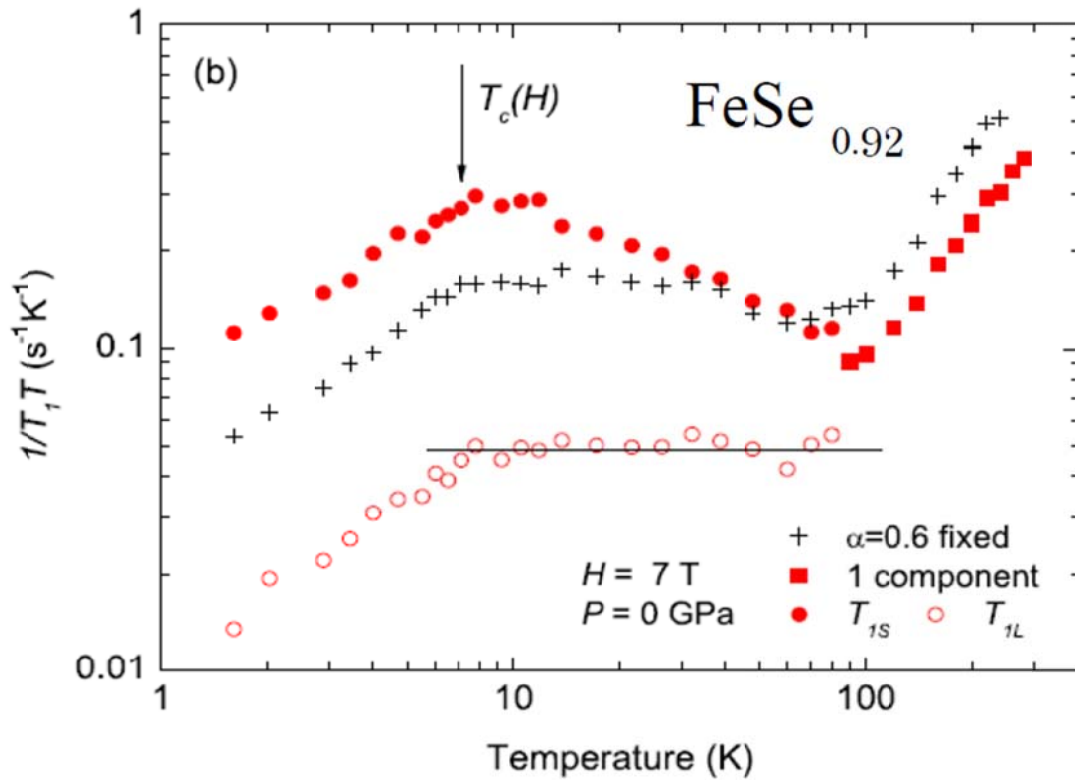
Masaki *et al.*, JPSJ **78**, 063704 (2009)

Figure 4-11b. Masaki et al. used different fitting functions, stretched exponential fitting and two-T_1 fitting, to their $FeSe_{0.92}$. Note that $1/T_{1S}T$ increases below 100 K, indicating the development of spin fluctuations. In contrast, $1/T_{1L}T$ is temperature-independent. For comparison, $1/T_1T$ deduced by fixing $\alpha = 0.6$ is also plotted [6].

4.5 NMR Spectra of Cu-doped $(Fe_{1-x}Cu_x)Se_{1-\delta}$

We have measured the ^{77}Se and ^{63}Cu NMR spectra and compared the difference between different Cu doping level of $(Fe_{1-x}Cu_x)Se_{1-\delta}$.

4.5.1 ^{77}Se NMR spectra of Cu-doped $(Fe_{1-x}Cu_x)Se_{1-\delta}$

Figure 4-12 shows the ^{77}Se NMR spectra in the normal state of $(Fe_{1-x}Cu_x)Se_{1-\delta}$ at 15 K, where the linewidth increases rapidly upon Cu doping and then saturates. This implies that Cu substitution induces a magnetic moment so that the line broadening is dominated by magnetic disorder, rather than by structural disorder. Judging by the rapid increase in ^{77}Se NMR linewidth, the disorder effects may or may not correlate with the rapid suppression of T_c by Cu doping.
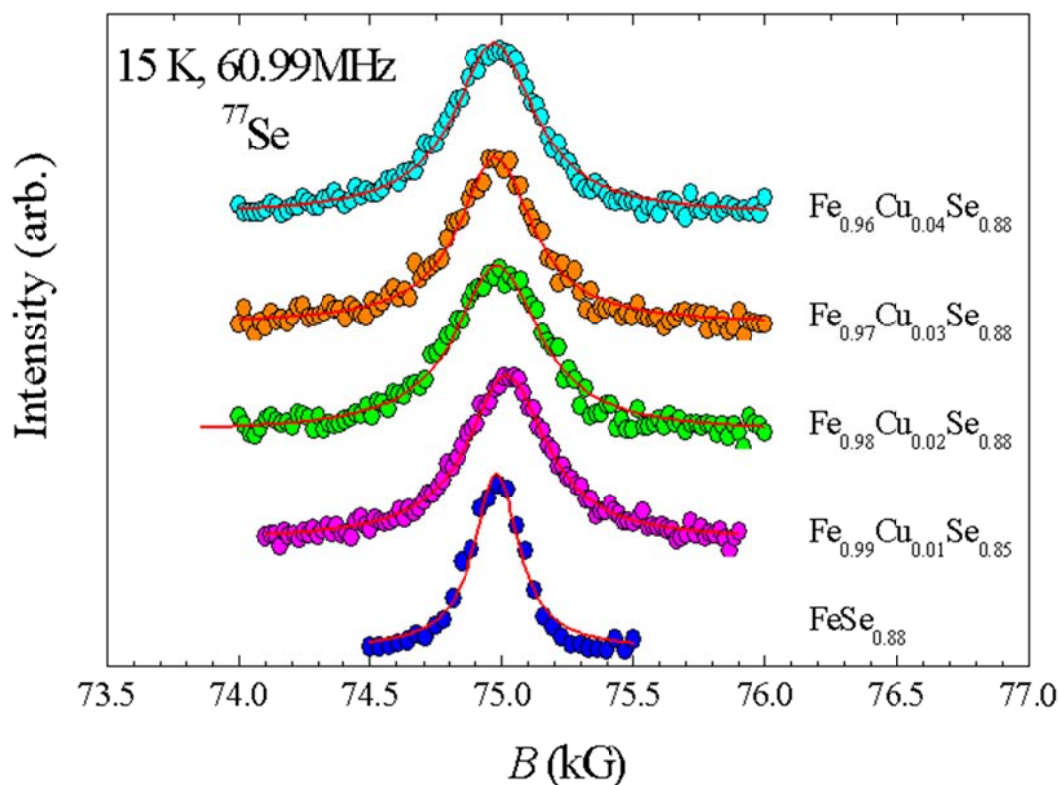

Figure 4-12. ^{77}Se NMR spectra, in the normal state of $(Fe_{1-x}Cu_x)Se_{1-\delta}$, at 15 K and 60.99 MHz.

4.5.2 ^{63}Cu NMR spectra of $(Fe_{1-x}Cu_x)Se_{1-\delta}$

Figure 4-13a is the plot of ^{63}Cu NMR spectra. Compare with the ^{77}Se NMR spectra of $(Fe_{1-x}Cu_x)Se_{1-\delta}$, the ^{63}Cu linewidth in figure 4-13 gradually decreases with the content of Cu doping suggesting that the induced moments are not at the Cu sites but at Fe sites.

From ^{63}Cu NMR spectra, we found that an important information that the central peak of spectra sharpened at higher Cu doping level due to the weakened transferred hyperfine field caused by the change in electric density of states in $(Fe_{1-x}Cu_x)Se_{1-\delta}$. This data can be examined the resistivity measurement.

Figure 4-13b is a different case where the growing linewidth caused by structural disorder in $TiFe_{1-x}Co_x$. Compare the two different examples. Although their linewidths both gradually growing bigger, the mechanisms behind are quiet different.

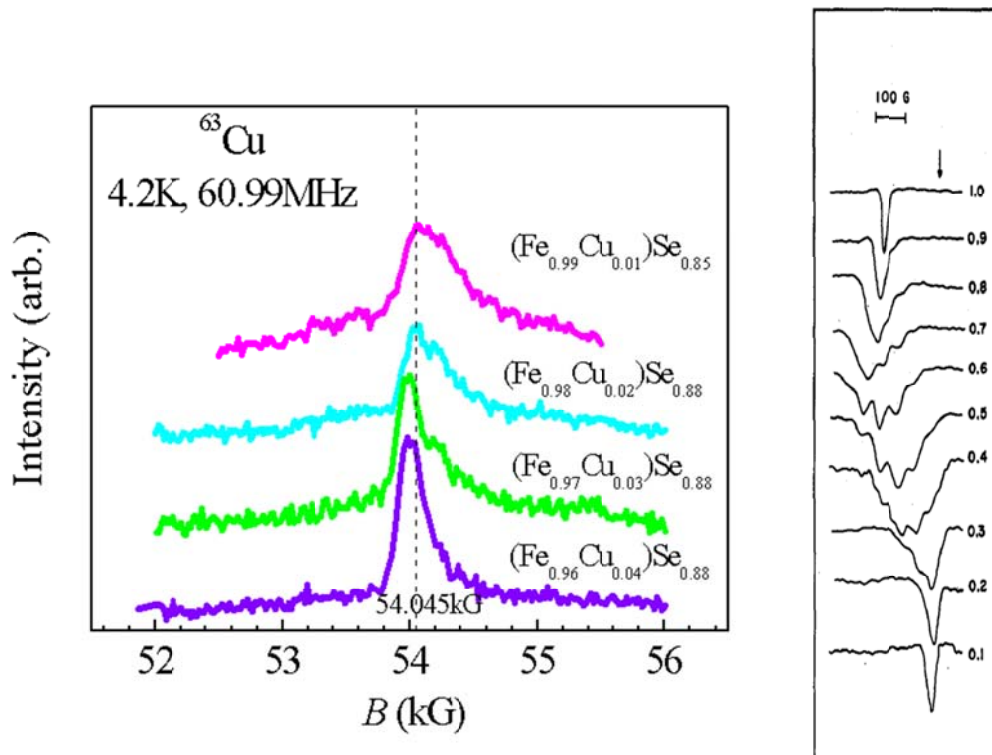**Figure 4-13a&b.** a is ^{63}Cu NMR spectra, in the normal state of $(Fe_{1-x}Cu_x)Se_{1-\delta}$,at 15 K and 60.99 MHz. Dashed Line is the reference field for the unshifted ^{63}Cu nucleus. The right (4-13b) is different doping in $TiFe_{1-x}Co_x$. Unlike the reason causing linewidth variation in the left (4-13a), the structural disorder effect causes different linewidth in $TiFe_{1-x}Co_x$. [12]

4.5.3 Comparison of ^{77}Se and ^{63}Cu NMR spectra of $(Fe_{1-x}Cu_x)Se_{1-\delta}$

Why do ^{63}Cu and 77Se linewidths behave so differently? Normally the NMR spectrum becomes wider and more asymmetric when the increase in doping level is begun [9, 10]. But here, the ^{63}Cu linewidth can come from both the doping-induced magnetic shift distribution, and the powder pattern due to the anisotropic shifts and quadrupolar effects. The broad shoulders, on both sides of the central peak, are caused by the quadrupolar broadening. Because these broad shoulders stay nearly unchanged, unlike the central peak sharpening at higher Cu doping, the quadrupolar effects probably do not cause the narrowing of the central peak. Note that the centroid of the spectrum moves closer to the unshifted reference line at higher Cu doping, implying that the Cu nuclei do not much feel the hyperfine fields, from the neighboring Fe/Cu spins, at a higher doping levels. Since there is no direct chemical bonding between the Cu and Fe atoms, part of the ^{63}Cu frequency shift at low Cu doping comes from the transferred hyperfine coupling, mediated by the conduction electrons. For higher Cu doping, we suspect that the metal-insulator transition reduces the number of conductions so that the transferred hyperfine coupling becomes weaker. Therefore, both the magnetic shift and linewidth decrease at higher Cu doping. This is different from the ^{77}Se spectra, where there is direct wave-function overlap between the 4p and Fe 3d electrons so that the ^{77}Se nucleus can always effectively probe the Fe spins, to show a broader linewidth at higher doping.

4.5.4 Linewidth and frequency shift of $(Fe_{1-x}Cu_x)Se_{1-\delta}$

Figure 4-14 is the phase diagram of Cu doping level to the linewidth and frequency shift of ^{77}Se NMR spectra. If we neglecting the zero doping point, we can see that the frequency shift (pink circles) jumps suddenly and then slowly increases with increasing Cu doping level. This infers that the line broadening is dominated by magnetic disorder induced by Cu doping, instead of structural disorder. We can see that the linewidth (blue circles) is nearly unchanged with Cu doping level. Similar line broadening in the Cu-doped samples that show different T_c suggests that disorder has little effect on the suppression of T_c.

Figure 4-14. Linewidth and frequency shift of the ^{77}Se NMR spectra.

4.5.5 Relation between T_c and disorder effect in $(Fe_{1-x}Cu_x)Se_{1-\delta}$

Figure 4-15 is the Cu doping level to the superconducting transition temperature, a superconducting phase diagram. We can see linewidth has no obviously direct connection to the superconducting transition. Similar line broadening in the Cu-doped samples that show different T_c suggests that disorder has little effect on the suppression of T_c.

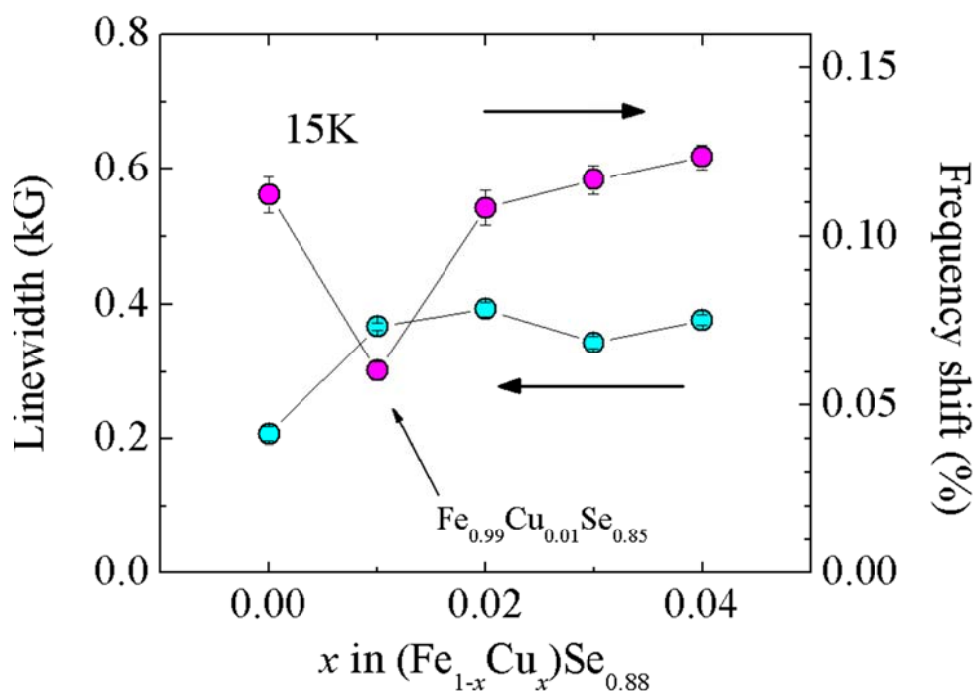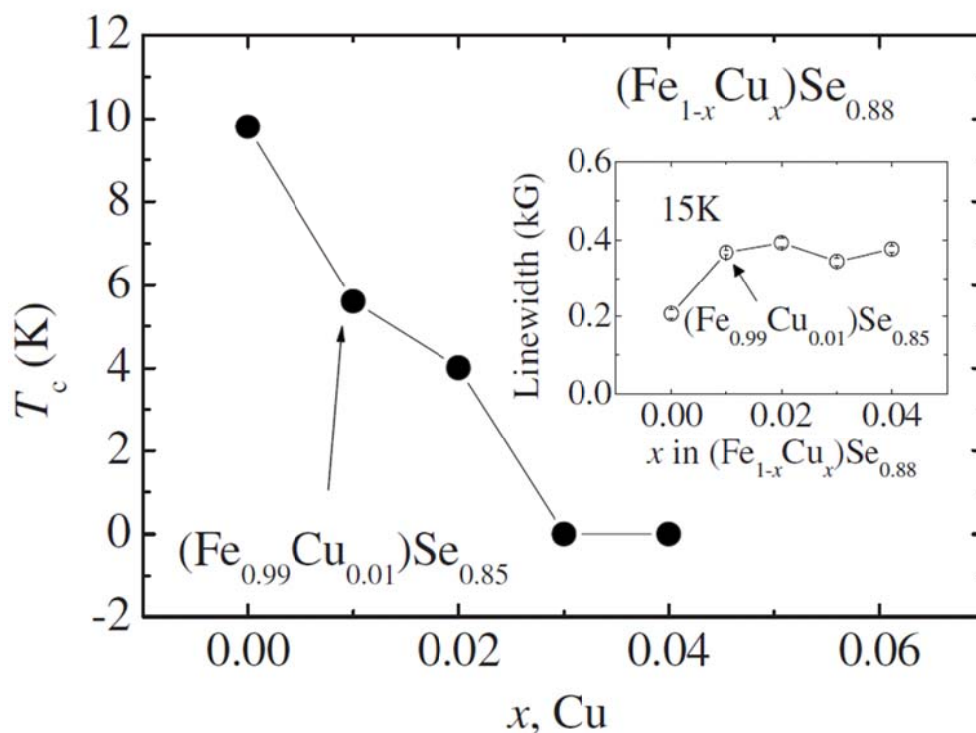**Figure 4-15.** Superconducting phase diagram of the Cu-doped FeSe. Inset: ^{77}Se NMR linewidth, as a function of Cu doping, at 15 K.

4.6 $1/T_1T$ of $(Fe_{1-x}Cu_x)Se_{1-\delta}$ by stretched exponential fitting

Figure 4-16 (blue circles) gives the average $1/(T_1T)$ data for our $FeSe_{0.88}$. Indeed, similar uprising behavior, at low temperature, is seen in our sample, in contrast to the flat behavior in the non-superconducting $FeSe_{0.97}$. Note that the drop of $1/(T_1T)$ below T_c, expected from the opening of the superconducting gap, is smeared out due to the broad $1/T_1$ distribution. The theory of calculating the average T_1 is from reference 8.
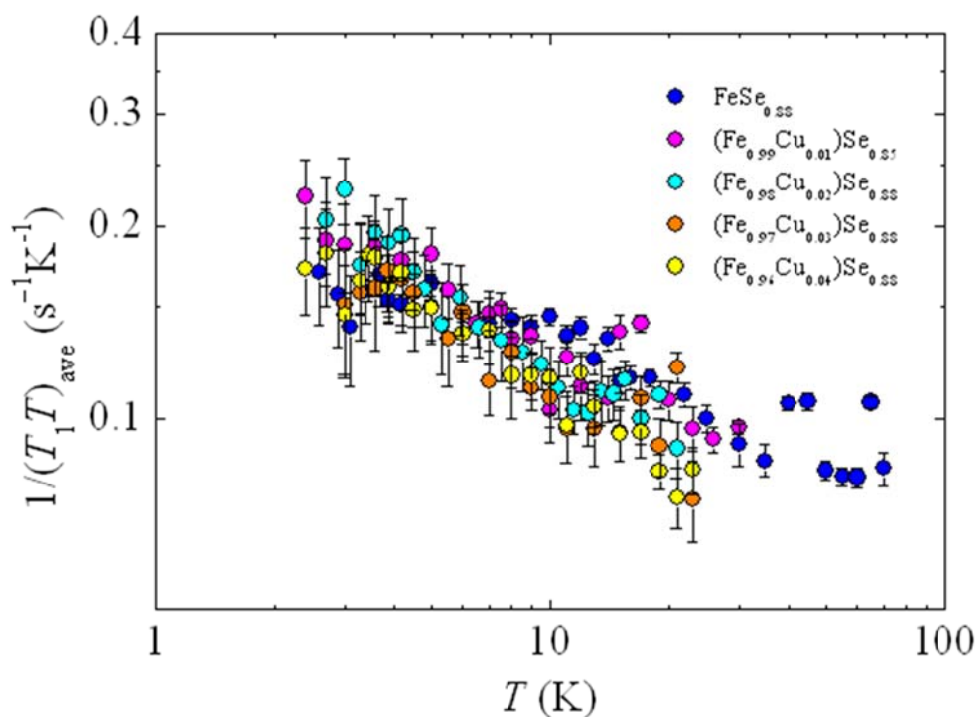

Figure 4-16. The average $(T_1T)^{-1}$, of ^{77}Se in $(Fe_{1-x}Cu_x)Se_{1-\delta}$, measured at 60.99 MHz (~75 kG). Note that a similar uprising behavior due to spin fluctuations is observed.

4.7 Conclusion & Summary

Combining the reduced superconducting volume fraction in the Se-deficient FeSe with the findings from the previous discussions, i.e., the different temperature-dependent $1/T_1$ at different Se sites and the reduced spin fluctuations at a larger δ, we infer that the Se-deficient FeSe has an inhomogeneous phase, where the superconductivity comes from regions with few or no Se vacancies. The Se-vacancy-free region has much stronger magnetic fluctuations than the Se-vacant region. When greater vacancy is introduced in FeSe, both the overall spin fluctuations and superconducting volume fraction will decrease. However, this picture cannot explain why the superconductivity disappears in $FeSe_{0.97}$ [7]. Is this really due to the oxygen contamination in those Se-deficient samples so that the superconductivity is actually from $FeSe_{1-\delta}O_y$, instead of $FeSe_{1-\delta}$? An oxygen-free $FeSe_{0.82}$ has been reported by Williams et al., with magnetic susceptibility clearly showing a superconducting diamagnetic response, if the background signal from the impurities is subtracted [3]. Therefore, we think it unlikely that occurrence of any oxygen contamination is the cause. While preparing this paper, we noticed that a different result was recently reported, where the superconductivity was claimed to exist in a narrow range of $\delta=0.03$, i.e., $FeSe_{0.974\pm0.005}$ [11]. These recent experiments, together with our own, indicate that the superconductivity emerges from the nearly stoichiometric FeSe. Figure 4-17 is the neutron diffraction data of different Se vacancy. From this, we know that the quantity of Se vacancy will only effect the composition phase content. Why do Imai et al. have a different result with M. K. Wu et al.? E. Pomjakushina says that Imai has an unnecessary quenching processing, which makes the structure is unstable. And this result an non-superconducting FeSe.

Sample name	Nominal composition	T_c (K)	Refined composition phase content (molar %)
LT085a	$FeSe_{0.85}$		$FeSe_{0.994(11)}$ ($P4/nmm$) 71.75 ± 1.75%
			Fe ($Im3m$) 26.23 ± 0.85%
			FeSe ($P6_3/mmc$) 2.02 ± 0.38%
LT085	$FeSe_{0.85}$	8.28	$FeSe_{0.963(5)}$ ($P4/nmm$) 86.38 ± 0.98%
			Fe ($Im3m$) 12.46 ± 0.33%
			FeSe ($P6_3/mmc$) 1.16 ± 0.18%
LT087	$FeSe_{0.87}$	8.34	$FeSe_{0.979(4)}$ ($P4/nmm$) 91.53 ± 0.91%
			Fe ($Im3m$) 7.70 ± 0.23%
			FeSe ($P6_3/mmc$) 0.77 ± 0.14%
LT092	$FeSe_{0.92}$	8.44	$FeSe_{0.976(4)}$ ($P4/nmm$) 94.50 ± 0.89%
			Fe ($Im3m$) 4.50 ± 0.21%
			FeSe ($P6_3/mmc$) 1.00 ± 0.13%
HT094	$FeSe_{0.94}$	8.21	$FeSe_{0.977(3)}$ ($P4/nmm$) 92.91 ± 0.70%
			Fe ($Im3m$) 6.36 ± 0.16%
			FeSe ($P6_3/mmc$) 0.73 ± 0.09%
LT096	$FeSe_{0.96}$	8.43	$FeSe_{0.978(4)}$ ($P4/nmm$) 96.02 ± 1.07%
			Fe ($Im3m$) 1.94 ± 0.23%
			FeSe ($P6_3/mmc$) 2.04 ± 0.19%
LT098	$FeSe_{0.98}$	8.21	$FeSe_{0.975(3)}$ ($P4/nmm$) 98.31 ± 0.59%
			Fe ($Im3m$) 0.57 ± 0.05%
			FeSe ($P6_3/mmc$) 1.12 ± 0.08%
LT100	$FeSe_1$	~8	$FeSe_{0.968(3)}$ ($P4/nmm$) 83.03 ± 0.61%
			Fe ($Im3m$) 0.46 ± 0.05%
			Fe_7Se_8 ($P3_121$) 16.51 ± 0.28%

Figure 4-17. Neutron diffraction of different Se vacancy of $FeSe_{1-x}$

As for Cu-doped $(Fe_{1-x}Cu_x)Se_{1-\delta}$, stretched exponential behavior is observed in the spin-lattice relaxation curves for all Cu-doped $(Fe_{1-x}Cu_x)Se_{1-\delta}$. The average $(T_1T)^{-1}$ curves are plotted in figure 4-16. Within experimental error, all of our samples show similar average $(T_1T)^{-1}$ behavior, where the values increasing at lower temperature. Interestingly, Cu substitution does not alter spin fluctuation in $FeSe_{0.88}$, though Cu^{2+} possesses a spin different from Fe^{2+}. We note that both superconducting volume fraction and T_c rapidly decreases, upon Cu doping. This is different from the Se-deficient samples, where only superconducting volume fraction reduces significantly. The similar superconducting volume fraction found in $(Fe_{0.99}Cu_{0.01})Se_{0.85}$ and $(Fe_{0.98}Cu_{0.02})Se_{0.88}$ could be an effect of compensation, due to the different values of x and δ. Recent transport experiments, on $(Fe_{1-x}Cu_x)Se_{1-\delta}$, have shown that increasing Cu doping migrates the metallic state to a Mott insulator[2,3]. Therefore, we suspect that the suppression of T_c is mainly due to the change in the electronic states rather than the spin dynamics.

In summary, we conducted comprehensive studies of the $_{77}$Se NMR in the Se-deficient and Cu-substituted FeSe. By comparing our data with previous literatures, we infer that $FeSe_{1-\delta}$ has inhomogeneous phases, where the superconductivity emerges from regions with little or no Se vacancy. As for the T_c suppression in $(Fe_{1-x}Cu_x)Se_{1-\delta}$, magnetic fluctuations are not directly relevant. We suspect that it is the electronic states changing by Cu substitution so that a metal-insulator transition arises and soon T_c is suppressed.
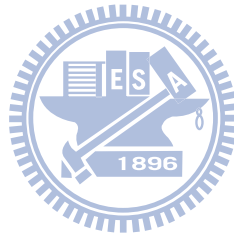
Appendix:

Personal designs of apparatus and programs

In the days of graduate study, my primary work is dedicating to develop laboratory automation. Our ultimate goal is to make all the NMR experimental measurements automatic. As a matter of fact, we already have some achievements. I have made several programs and apparatus for my master study. All of them are for NMR experimental research and the experimental equipment operation, such as experimental data acquisition, liquid helium compression, helium gas recovery and recycling, etc. The following is the list of apparatus and related programs that I made for our NMR experiments.

Apparatus

Homemade 5-Axis DC motor drive

The 5-Axis DC motor drive is computer-controlled by our Labview program. It consists of a power module and a motor control module. I utilize SANYO's LB1640N, a motor drive IC, to control our DC motors. The motor control module is a circuit composed of 5 LB1640N ICs, so it can drive 5 DC motors. By the basic PWM (Pulse Width Modulation) technique, we can even decide the motor's rotational speed. Due to technical difficulties, it's hard to control the motor's driving voltage directly in the past, so the PWM technique emerges and solves this problem successfully. Nowadays, PWM is a well-developed engineering technology and widely used in automatic control system. LB1640N is an H-bridge circuit IC, and we can directly control it by just two ports. By TTL signal, it can move and stop right away. With National Instrument's digital input/output controller, USB-6501, which converts the USB signal to 24 digital high/low output, we can control our motor drive through a corresponding program written with Labview. The motor drive controls lots of our instruments, such as the needle valve, variable capacitors, vacuum Regulator, etc.

Helium gas bag volume detector

We use a water level switch as the helium gas bag volume detector. The helium gas recycle system is composed of several parts. One of them is the helium gas bag volume detector. When the gas bag is full, the detector will close the electric valve. Then we control the inlet and outlet of the gas bag. All the operation is done by National Instrument's Labview program on PC, and it controllable remotely (via internet).
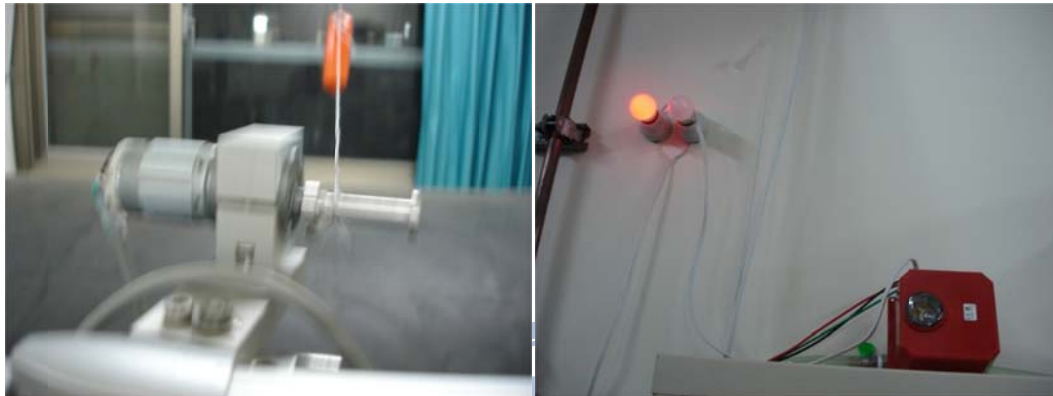
NQR temperature control system

The temperature control system of the nuclear quadrupole resonance experiment is composed of three parts, which are a liquid nitrogen Dewar, a temperature controller, and a linear motion stage. The temperature controller is Lakeshore 336 containing four temperature sensor ports and two heater output. Lakeshore 336 utilizes the PID technique, which can accurately control the temperature. A proportional integral derivative controller (PID controller) is a generic control loop feedback mechanism (controller) widely used in industrial control systems – a PID is the most commonly used feedback controller. A PID controller calculates an "error" value as the difference between a measured process variable and a desired setpoint. The controller attempts to minimize the error by adjusting the process control inputs. In the absence of knowledge of the underlying process, PID controllers are the best controllers. However, for best performance, the PID parameters used in the calculation must be tuned according to the nature of the system – while the design is generic, the parameters depend on the specific system. The length of the motion stage is 70 cm, which can control the NQR probe's position. The position of the probe decides the cooling rate, and Lakeshore 336 controls the heating rate. The balance of heating and cooling rate determines the final temperature. Both of them have corresponding programs.

Remotely control Evaporative cooling system

The evaporative cooling system is set up by Professor Ben-Li Young. What I did is designing a DC motor and a connecting device on the vacuum regulator so that we can control it remotely. Evaporative cooling is commonly used in cryogenic experiments. The vapor above a reservoir of cryogenic liquid is pumped away, and the liquid continuously evaporates as long as the liquid's vapor pressure is significant. Evaporative cooling of ordinary helium can cool to at least 1.2K. This technique can be used to make cryocoolers. As the temperature decreases, the vapor pressure of the liquid also falls, and cooling becomes less effective. We utilize LJ-engineering model 329, vacuum regulator, as our pumping rate controller so that we can dominate the temperature of our NMR experiment. With the temperature controller Lakeshore 332, we can change the temperature through changing the vacuum regulator rotated by the DC motor, which is controlled by the PC program. So we can do all the experiments remotely.

Labview Programs

DC motor controller

The DC motor controller utilizes the PWM technique, which controls the rotary speed of the motor. The program can make the motor move forward and backward and record its position at the same time. The program is written with National Instrument's Labview, a visual programming language.
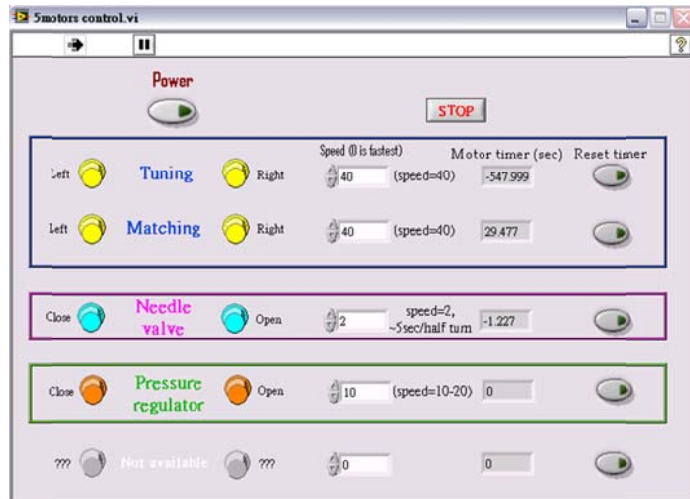
Hewlett-Packard 8752C & 8712ET RF Network analyzer

The HP 8752c network analyzer can show the resonance frequency of the LC circuit. A network analyzer is an instrument used to analyze the properties of electrical networks, especially those properties associated with the reflection and transmission of electrical signals known as scattering parameters (S-parameters). In NMR experiment, the network analyzer is used to confirm that the resonance frequency of LC circuit in the NMR probe is right. I write a program demonstrating the reflection rate of LC circuit in the probe. With another tuning and matching program I wrote, the resonance frequency can be any value we want. The program is written with National Instrument's Labview, a visual programming language.
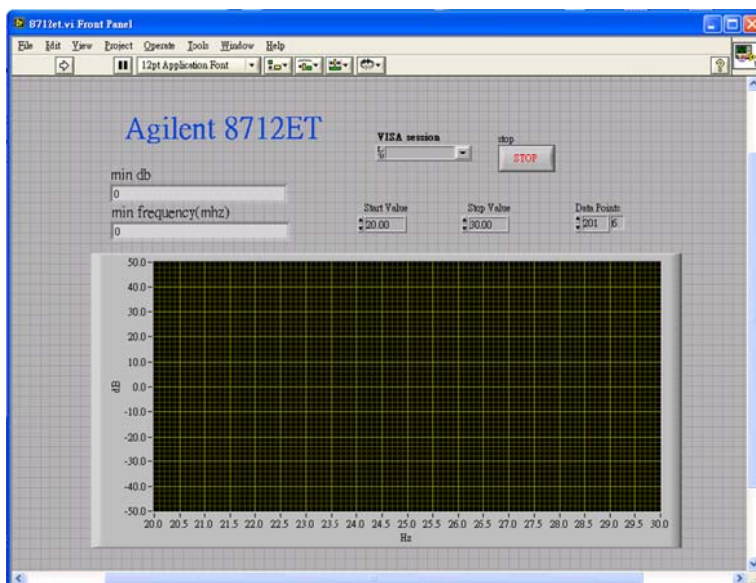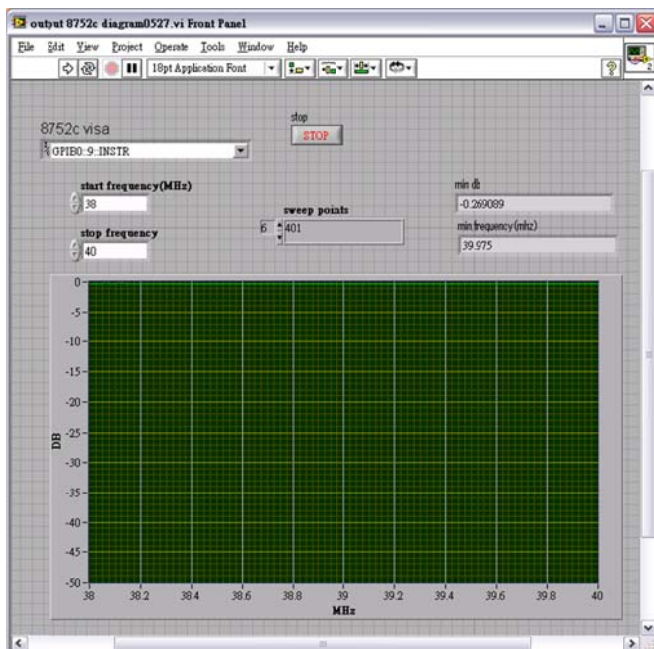
CS4 Superconducting Magnet Power Supply

The CS4 controller is a power supply controlling the applied magnetic field of the NMR experiment. The program is has several security mechanism preventing it from the operation error. If we turn on the heater with an unequal current between the magnetic and the power supply, it will cause damage to the superconducting magnetic coil. The CS4 controller can safely tune the power supply to the designated magnetic field. It's connected to the computer with the GPIB interface. All the operation is done by the official command list. The program is written with National Instrument's Labview, a visual programming language.
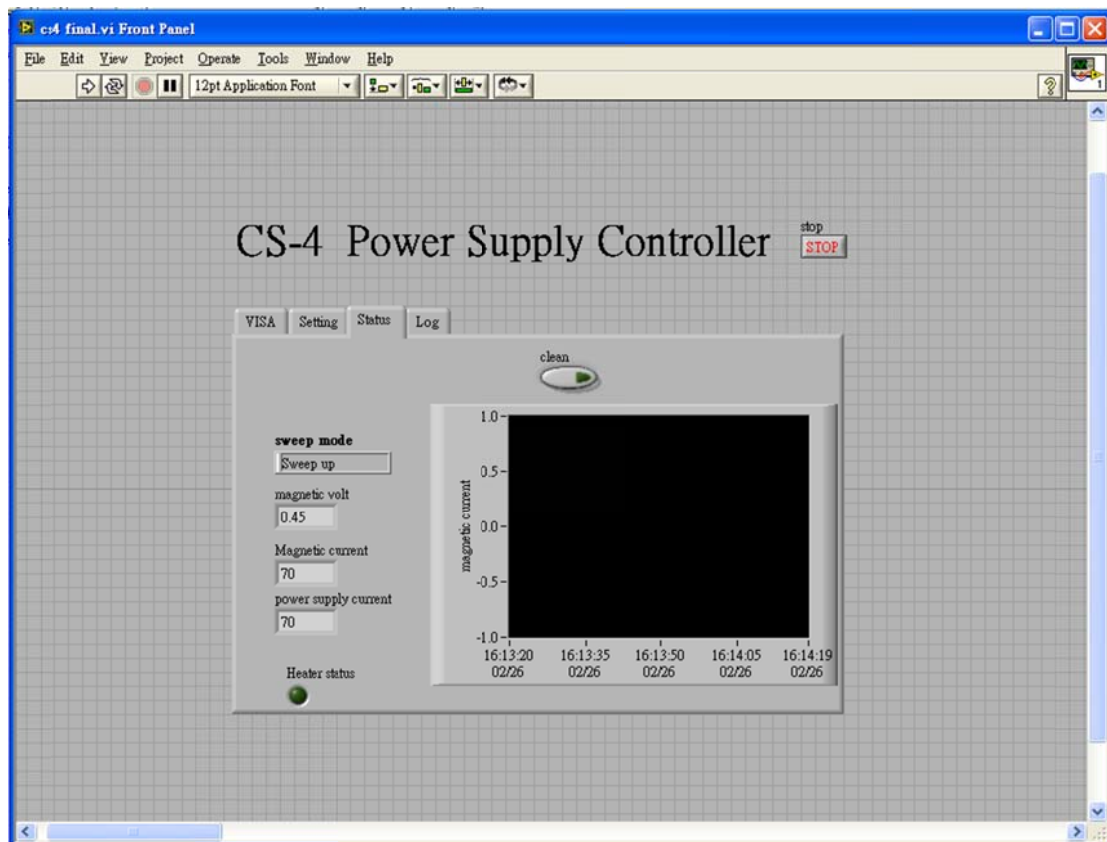
Liquid helium level monitor-LM500

Our NMR lab has two Liquid helium level monitor, one is for the superconducting magnetic Dewar, Janis, and the other is for the Liquid Helium container. I wrote this program so that I can read the level of liquid helium remotely. The liquid helium level monitor LM500 is connected to the computer with RS232 interface. All the operation is done by the official command list. The program is written with National Instrument's Labview, a visual programming language. It has the function of saving data and plotting the liquid helium level showing the trend of the consuming of liquid helium.
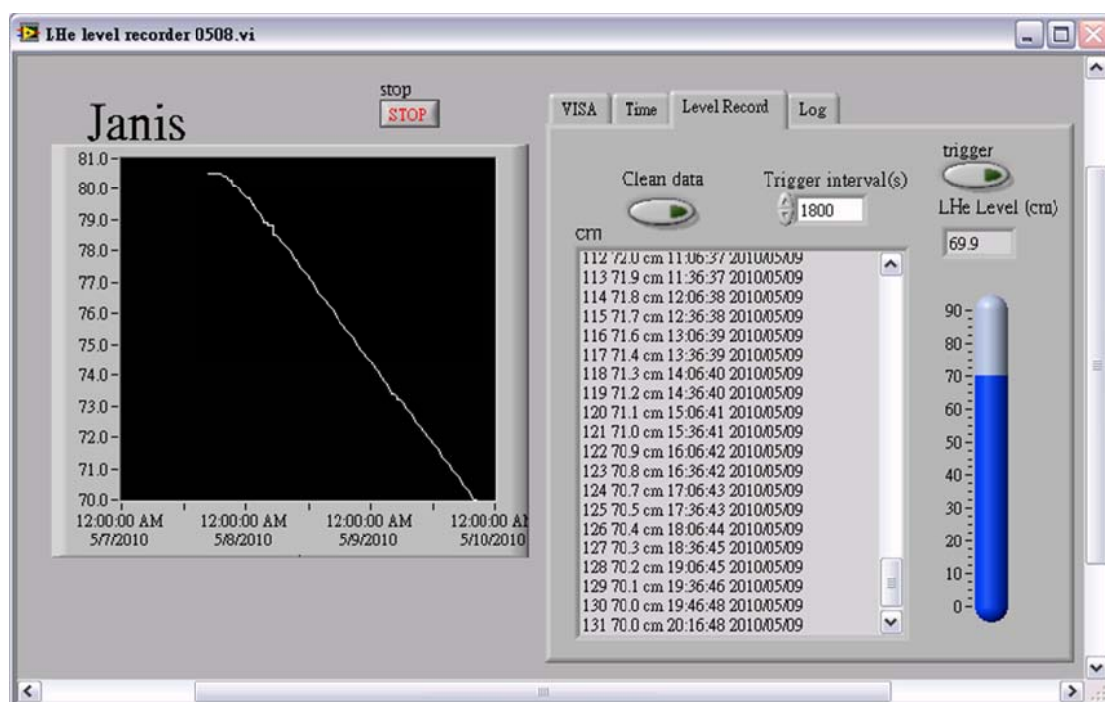
Liquid helium compressor, LHeP12

The NMR experiment consumes a large amount of liquid helium, so the evaporating helium gas will be recycled to the recycling gas bag. Then the compressor will compress the gaseous helium into liquid state. This program monitors the machine status. By appropriate parameters, the compressor will work in the optimal way. Additionally, it also has the saving data function, and it can record the time that starts or stops compressing. The program is written with National Instrument's Labview, a visual programming language.
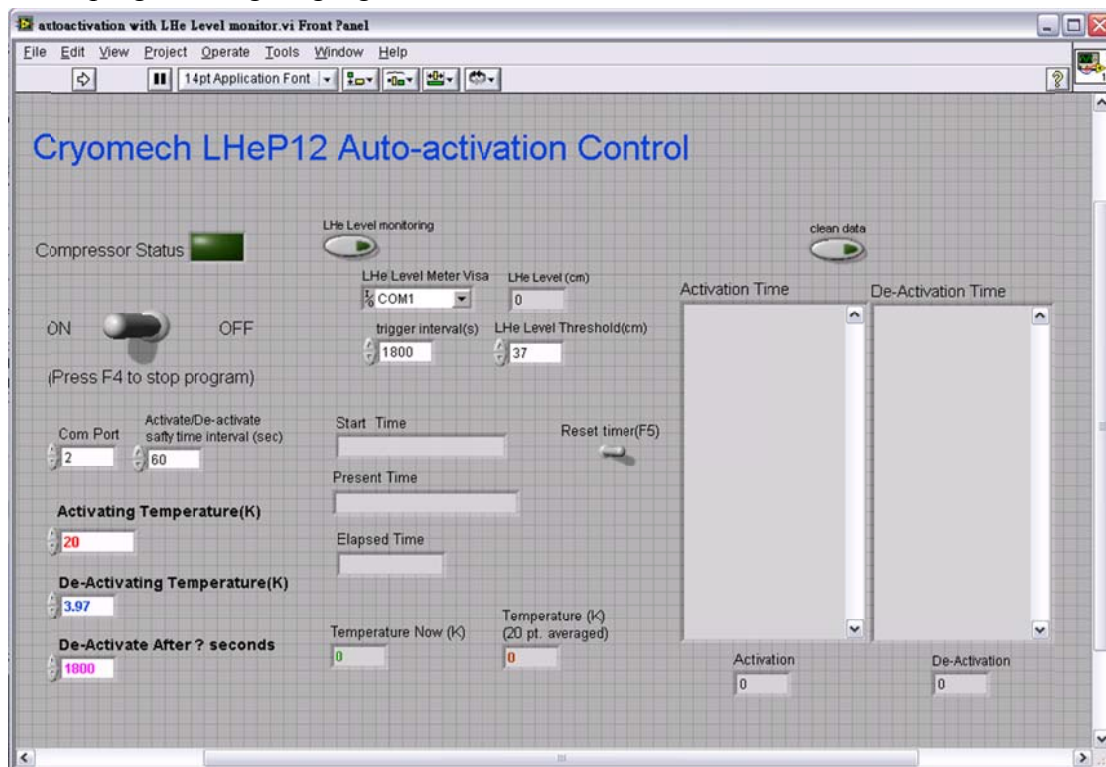
Temperature controller-Lakeshore 336

The temperature controller, Lakeshore 336, is available with four inputs and two heater output. The program can choose the control input channel and heater output channel, which are the necessary parameters for temperature. While selecting the right channels, we still need to choose the PID mode. The intelligent auto-tuning feature of Lakeshore 336 can be used to automatically collect PID parameters, which makes us spend less time tuning your controller and more time conducting experiments. But we can also use the manual mode, whether manual PID mode or purely manual mode. Just like others, the program has the function of saving data and drawing the temperature-time diagram showing the trend of the changing rate of the temperature. This program is written with National Instrument's Labview, a visual programming language.
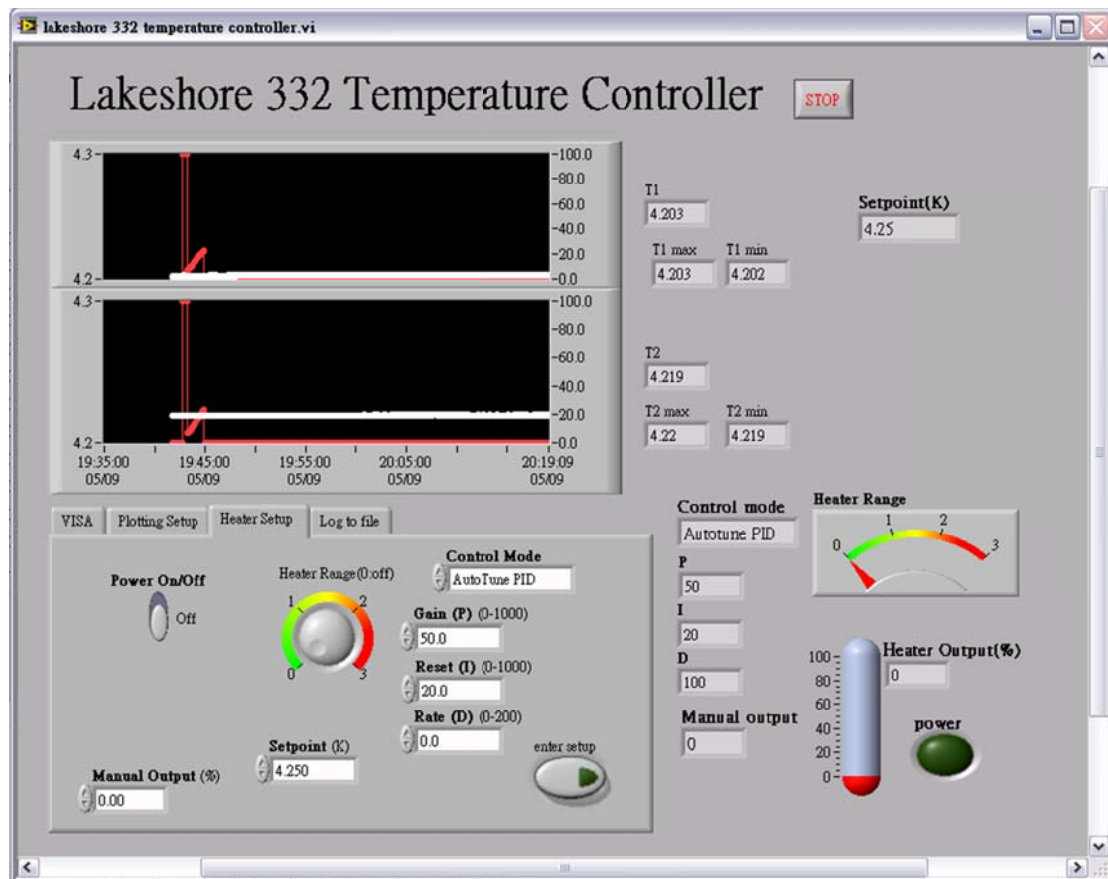
Temperature controller-Lakeshore 332

Mostly same as Lakeshore 336, the program of Lakeshore 332 has same functions. The difference between these two temperature controllers are that Lakeshore 332 only has one heater out and they don't use the same controlling commands. This program is written with National Instrument's Labview, a visual programming language.
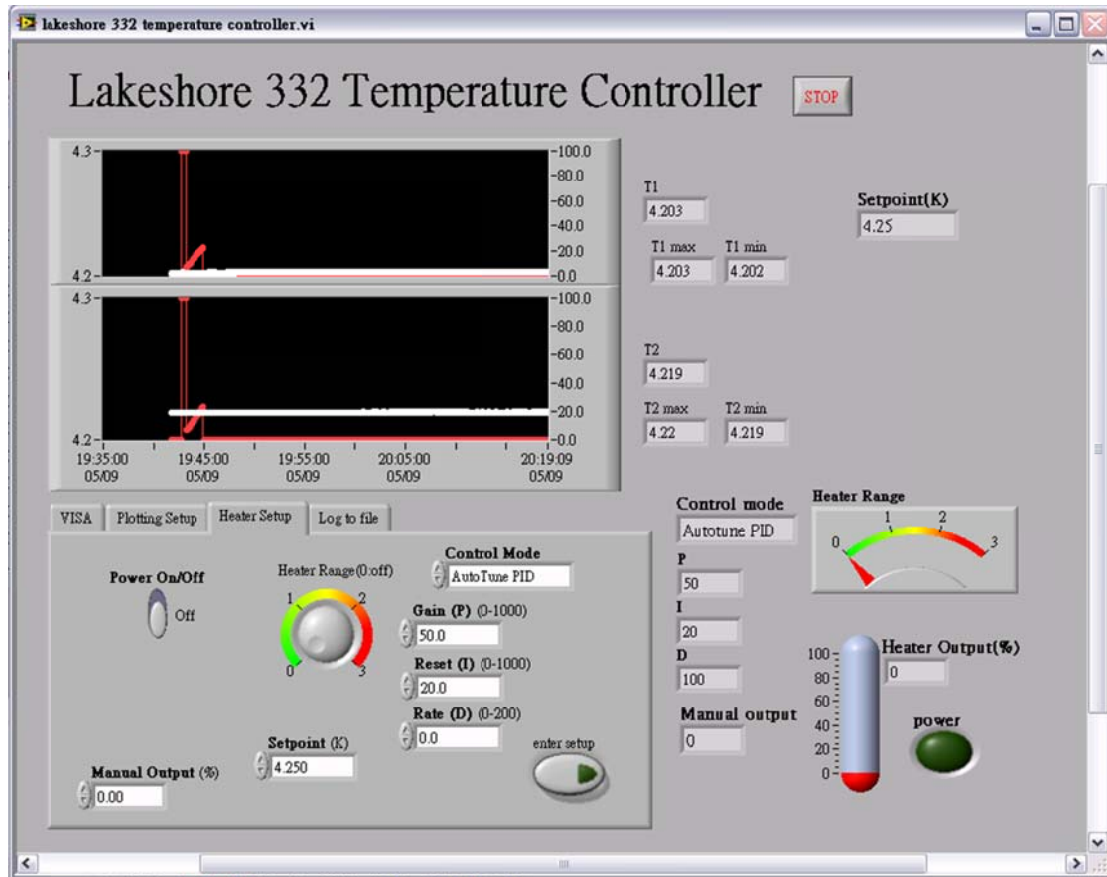
Motion stage controller

The program of the motion stage is to control the cool rate of the NQR experiment's temperature. The NQR probe is stuck to the stage, and the probe is in the liquid nitrogen dewar. We change the depth of the NQR probe in the dewar so that we can determine the cooling rate of the temperature controlling system. The program has two modes, relative moving and absolute moving. Absolute moving can make the probe go to a designed position, and relative moving can move the probe by the direction we choose. This program is written with National Instrument's Labview, a visual programming language.
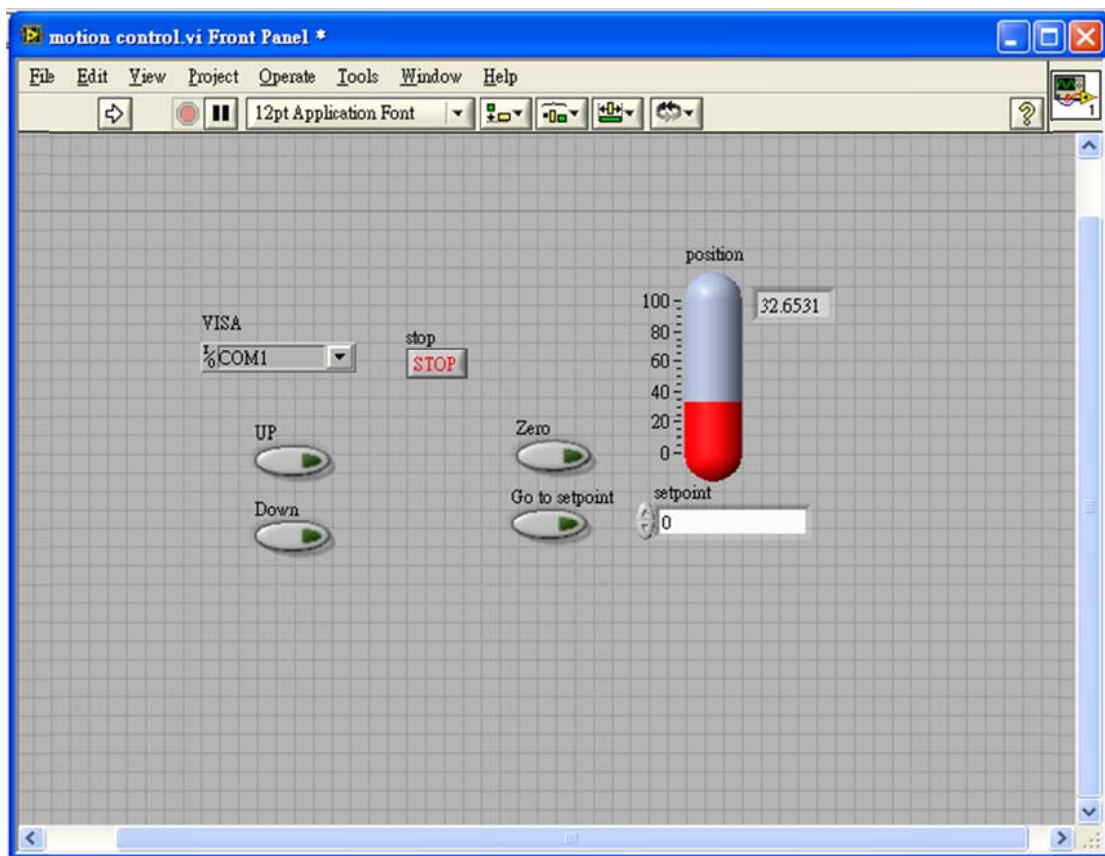
AC susceptibility experiment (magnetic field sweep)

The program records the magnetic field and the resonance frequency of the LC circuit of the NQR probe, which reflects the susceptibility of the measured sample in the probe. We can determine the field of magnetic phase transition (if the sample has it). All the safety mechanism of the superconducting magnetic is considered. The function of saving data for analyzing is included, and we can also read it from the frequency-B diagram drawn by the program. By the data, we can plot a phase diagram. This program is written with National Instrument's Labview, a visual programming language.
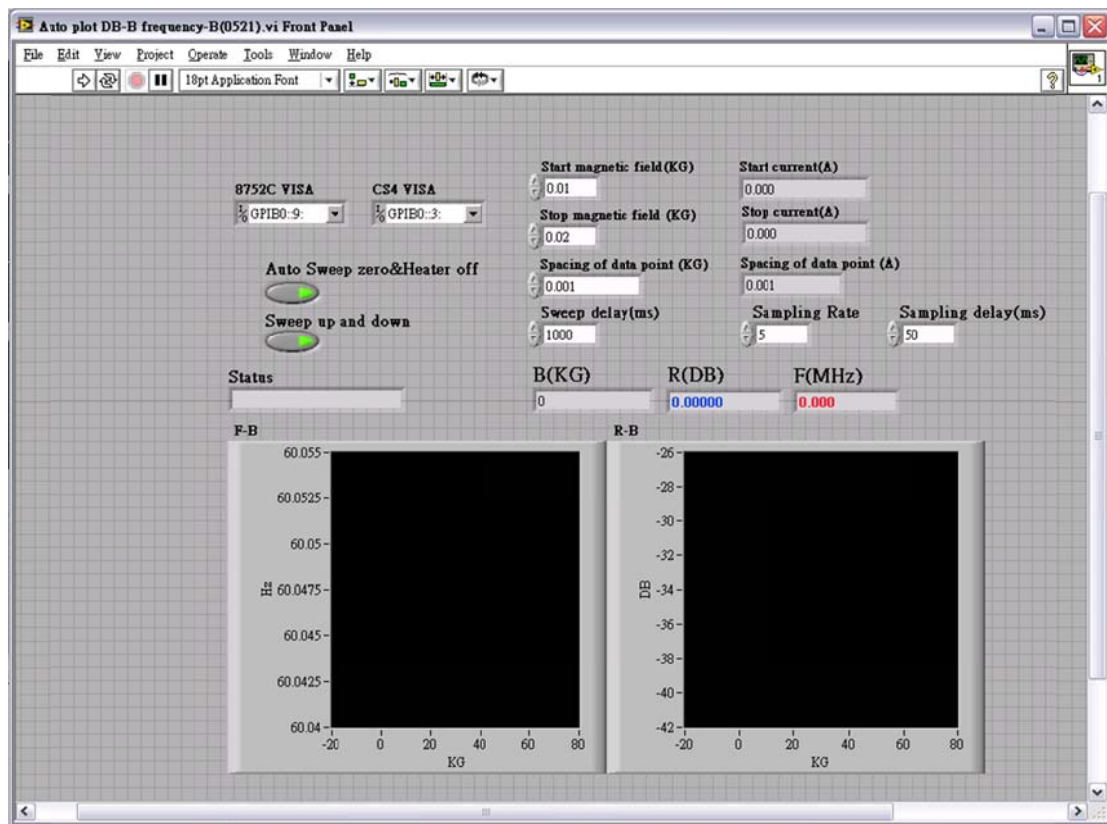
AC susceptibility experiment (temperature sweep)

The program records the temperature and the resonance frequency of the LC circuit of the NMR probe, which reflects the susceptibility of the measured sample in NMR probe. By this experiment, we can determine the phase transition temperature, such as structure and superconducting transition. By the way, we can further estimate the superconducting volume fraction (if the sample is a superconductor), but the value is not that accurate. We can only take it as a reference value. Same as the magnetic field sweep's program, the function of saving data for analyzing is included, and we can also read it from the frequency-temperature diagram drawn by the program. By the data, we can plot a phase diagram. This program is written with National Instrument's Labview, a visual programming language.
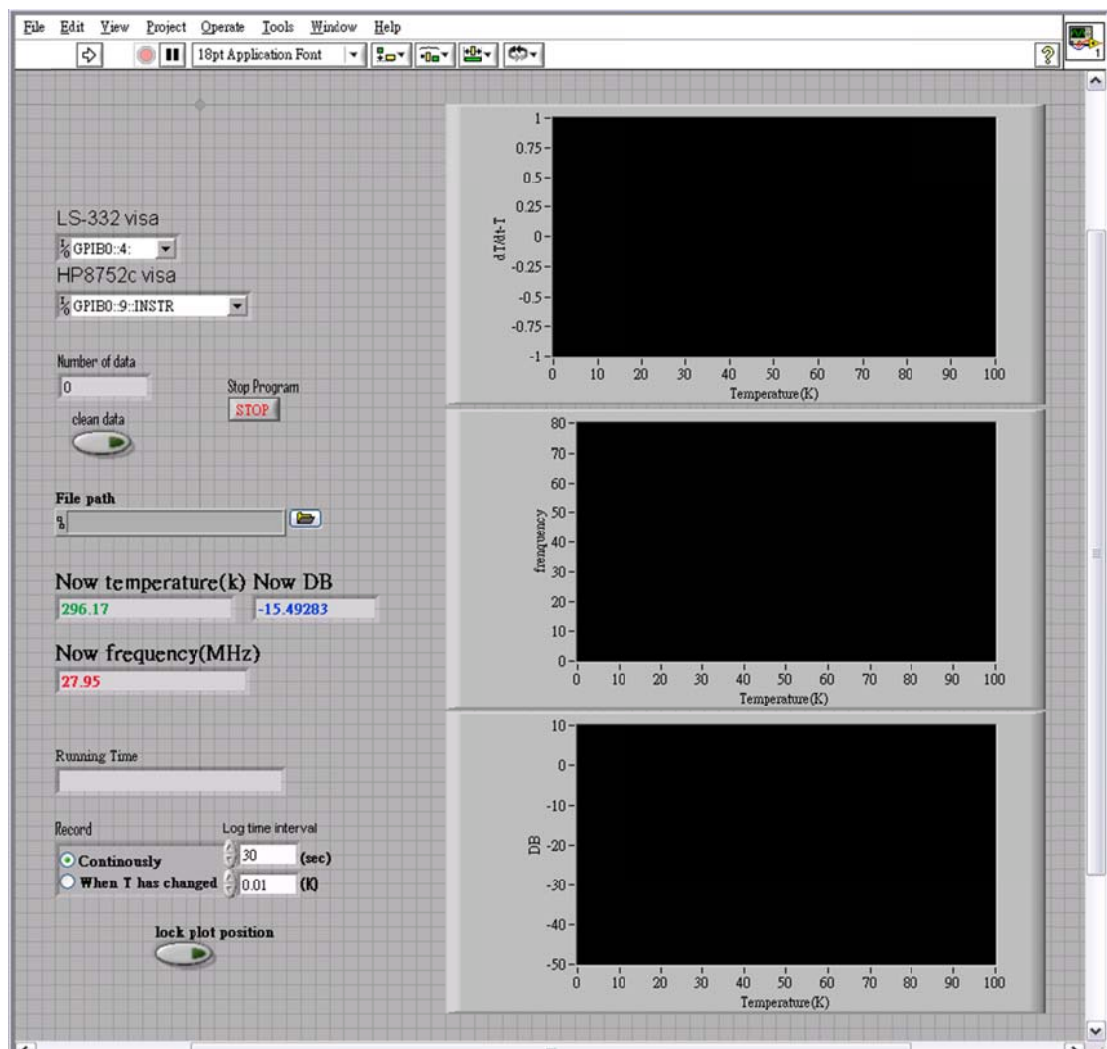
Agilent 8648A signal generator

We want to control the signal generator remotely, so I wrote a labview program for Agilent 8648. We can change the frequency and magnitude by the labview program.
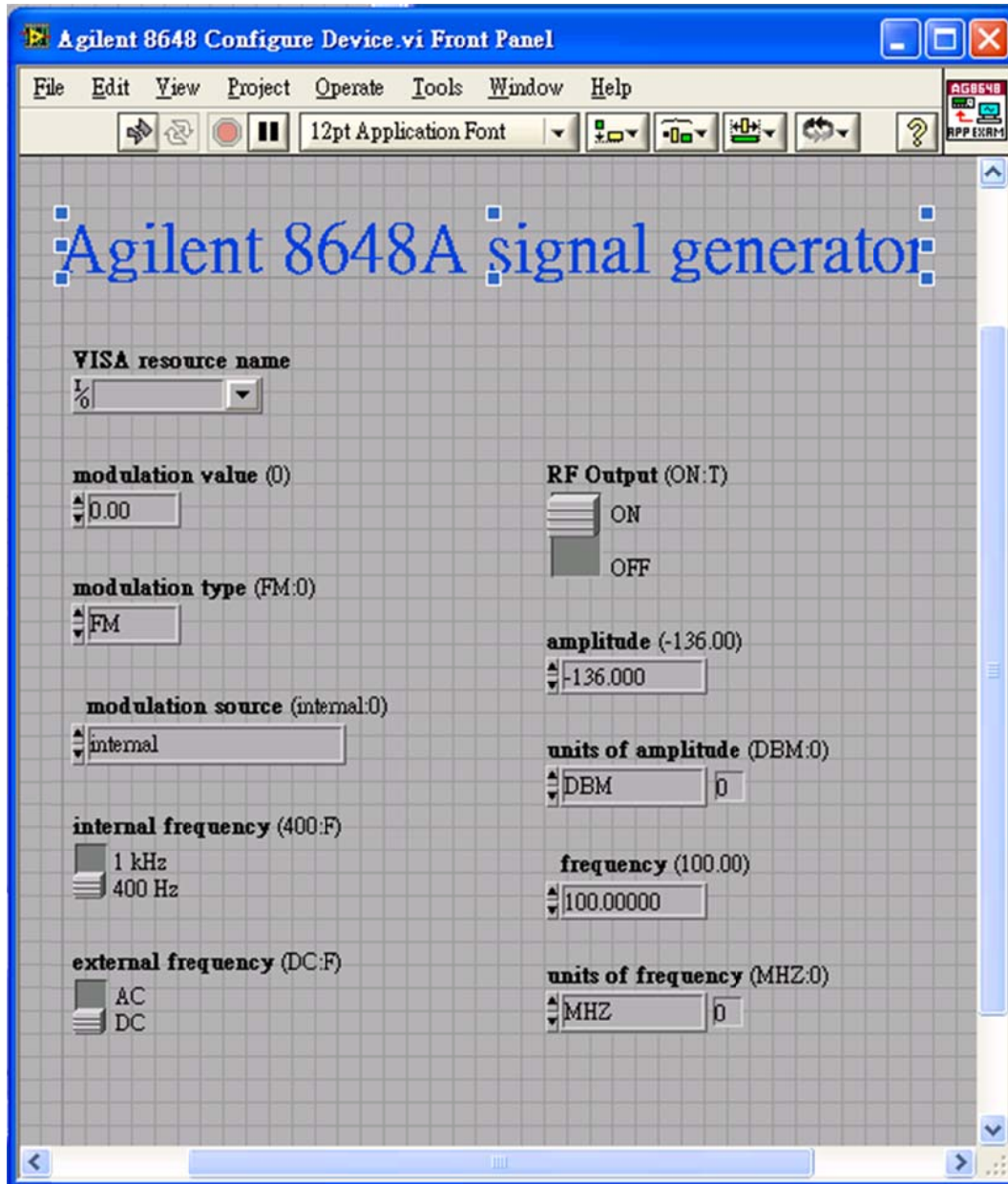
Tektronix TDS 2022B oscilloscope

We can see the waveform of the signal from the Tektronix TDS 2022B oscilloscope via the National Instrument's signal express program. We can also tune the parameters, such as …......

For the NMR experiment, we want to know the quality of the pulse exciting the sample. The quality of pulse is very easy to be effected by the transmitting circuit between the NMR probe and the spectrometer. We need to tune the pulse by the NMR controlling program. Through the program, we can observe the signal quality remotely and change the parameter of pulse immediately.
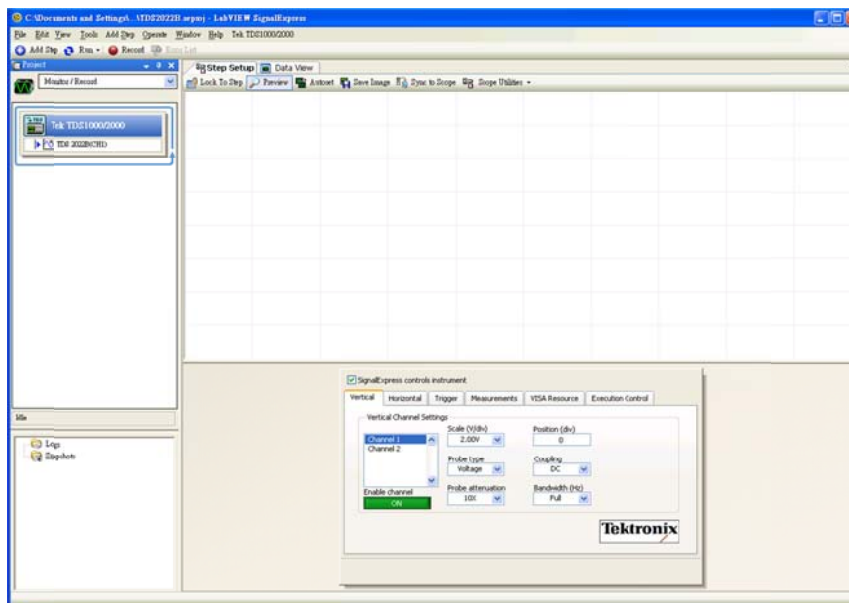
Agilent 54642 oscilloscope

We can see the waveform of the signal from the Agilent 54642 oscilloscope. We also want to see it remotely via computer, so I write a Labview program for controlling the scope remotely.

For the NMR experiment, we want to know the quality of the pulse exciting the sample. The quality of pulse is very easy to be effected by the transmitting circuit between the NMR probe and the spectrometer. We need to tune the pulse by the NMR controlling program. Through the program, we can observe the signal quality remotely and change the parameter of pulse immediately.
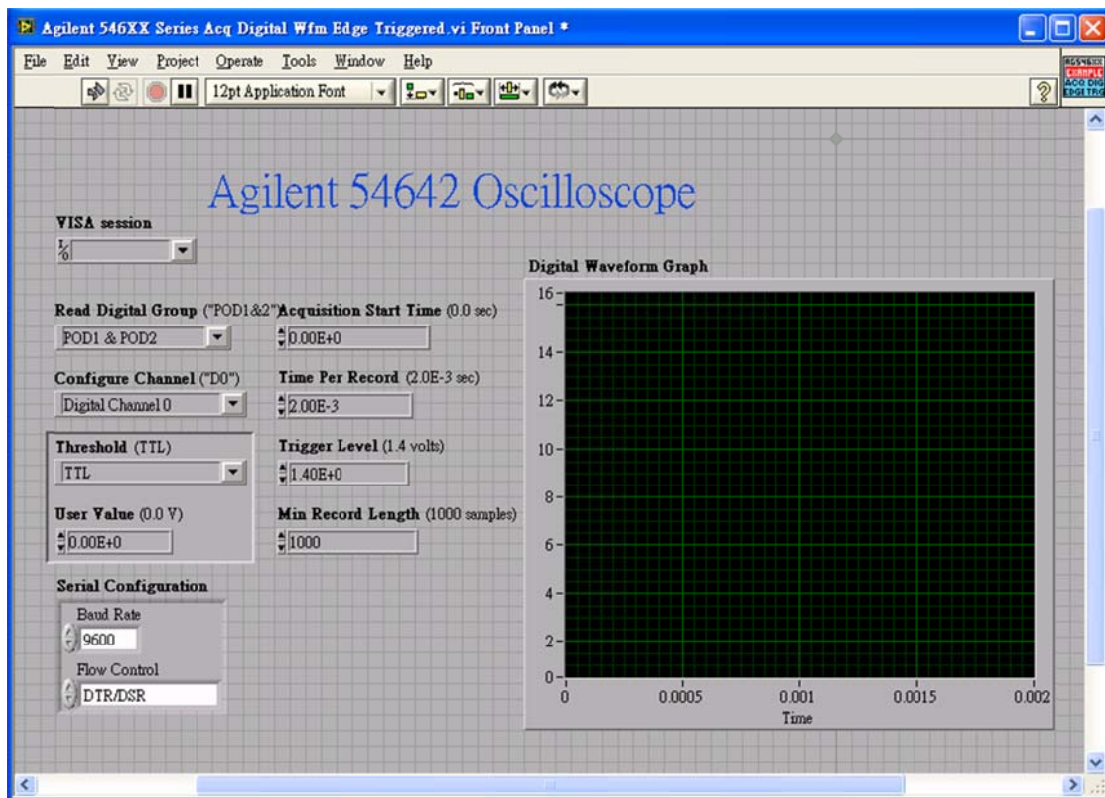
Reference

Ch1. Introduction

1. Yoichi Kamihara et al.,” Iron-Based Layered Superconductor: LaOFeP”, <u>Journal of the American Chemical Society</u>, 128(31), pp.10012-10013, July 2006.

2. Yoichi Kamihara et al.,” Iron-Based Layered Superconductor La[O$_{1-x}$F$_x$]FeAs (x = 0.05−0.12) with Tc = 26 K”, <u>Journal of the American Chemical Society</u>, 128(31), pp.3296-3297, February 2008.

3. Marianne Rotter et al.,” Superconductivity at 38 K in the Iron Arsenide (Ba$_{1-x}$K$_x$)Fe$_2$As$_2$ ”,<u>Physical Review Letters</u>,101,107006,September 2008.

4. Joshua H. Tapp et al.,” LiFeAs: An intrinsic FeAs-based superconductor with Tc=18K”, <u>Physical Review B</u>, 78, 060505, August 2008.

5. F.C. Hsu et al.,” Superconductivity in the PbO-type structure alpha-FeSe”, PNAS, 105, pp.14262-14264, September 2008.

6. S. Medvedev et al., Nature Materials 8, 630 (2009)

7. S. Margadonna et al., Chem. Commun. p.5607 (2008)

8. A. Subedi et al., Phys. Rev. B 78, 134514 (2008)

9. M. V. Sadovskii, Phys.-Usp. 51, 1201 (2008)

10. M. H. Fang et al., Phys. Rev. B 78, 224503 (2008)

11. T. Imai et al., Phys. Rev. Lett. 102, 177005 (2009)

12. S. Masaki et al., J. Phys. Soc. Jpn. 78, 063704 (2009)

13. Y. Mizuguchi et al., Appl. Phys. Lett. 93, 152505 (2008)

14. T. M. McQueen et al., Phys. Rev. B 79, 014522 (2009)

15. T. Huang et al., arXiv:0907.4001 (unpublished)

16. A. J. Williams et al., J. Phys.: Condens. Matter 21, 305701 (2009)

Ch2. NMR theory

1. N J Curro, "Nuclear magnetic resonance in the heavy fermion superconductors", Rep. Prog. Phys. 72 (2009) 026502 (24pp)
2. Charles P. Slichter, "Principles of magnetic resonance", Springer series in solid-state sciences (1996)
3. Eiichi Fukushima and Stephen B.W. Roeder, "Experimental pulse NMR: A nuts ana bolts approach", Addison-Wesley publishing company(1981)

Ch3. NMR experimental methods and instruments

1. E. L. Hahn, Phys. Rev. 80, 580–594 (1950)
2. James Keeler, "Fourier transformation and data processing", Understanding NMR Spectroscopy(2002)

Ch4. Experimental Process and Results

1. M. K. Wu et al., Physica C 469, 340 (2009)
2. T. Huang et al., arXiv:0907.4001 (unpublished)
3. A. J. Williams et al., J. Phys.: Condens. Matter 21, 305701 (2009)
4. T. Imai et al., Phys. Rev. Lett. 102, 177005 (2009)
5. H. Kotegawa et al., J. Phys. Soc. Jpn. 77, 113703 (2008)
6. S. Masaki et al., J. Phys. Soc. Jpn. 78, 063704 (2009)
7. T. M. McQueen et al., Phys. Rev. B 79, 014522 (2009)
8. C. P. Lindsey & G. D. Patterson, J. Chem. Phys. 73, 3348 (1980)
9. L. J. Swartzendruber et al., J. Appl. Phys. 39, 2215 (1968)
10. G. Papavassiliou et al., Phys. Rev. B 66, 140514(R) (2002)
11. E. Pomjakushina et al., Phys. Rev. B 80, 024517 (2009)
12. L. J. Swartzendruber, J. appl. phys., 39(1968), 2215

Publication

1. Ben-Li young, Jack Wu, Tzu-Wen Huang, Kuo-Wei Yeh, and Maw-Kuen Wu, "Magnetic fluctuations in $FeSe_{1-\delta}$ and Cu doped $FeSe_{1-\delta}$: ^{77}Se NMR experiments", Physical Review